Discover Applied Sciences

Research

Statistical and sensitivity analysis of ultrasound signals for effective condition monitoring of electro-motors using industrial approach

Hamed Mobki[1] · **Ehsan Shabahang Nia**[1] · **Aydin Azizi**[2]

Received: 27 November 2023 / Accepted: 3 June 2024
Published online: 03 July 2024

Abstract
This paper researches the importance of ultrasound methodology for swiftly detecting faults in electric motors and rotating machines. The primary focus of this research is on the intricate signal processing of ultrasound signals from both faulty and fault-free electro-motors. The principal goal is to conduct a comprehensive statistical investigation into signal factors, examining the effects of defect progression on the factors associated with continuously operating faulty electro-motors. In addition to the statistical analysis, this study explores the envelope-frequency spectrum of the signal under both healthy and defective conditions, employing the envelope method alongside Hilbert transformation. The objective is to thoroughly scrutinize the dynamic changes in ultrasound waveform and envelope spectrum of defective states, considering diverse degrees of defect severity over an extended time span. Moreover, the paper meticulously tracks the trajectory of factor changes over a 40-day operational period of a defective electro-motor. Additionally, the study delves into the sensitivity of the ultrasound method to impulse-wise shocks, which are recurrently observed in ultrasound signals, leading to deviations in certain signal factors from their established healthy thresholds. In response to this challenge, this paper conducts a particular analysis of signal factor sensitivity to impulse-wise noises, identifying robust factors that serve as reliable tools for firm condition monitoring. These identified factors are then presented as invaluable contributors to ensuring the precision and reliability of condition monitoring, especially in the presence of disruptive impulse-wise noises.

Article Highlights

- Ultrasound's Crucial Role: This article delves into the pivotal role of ultrasound in monitoring the health of electric motors and rotating machines, highlighting its significance in detecting defects.
- Signal Analysis: The study initially focused on analyzing ultrasound signals from healthy and defective motors. The waveform differences between these states were examined, revealing distinct changes when defects were present. Notably, the emergence of intermittent impulses altered the waveform as defect severity increased.
- Severity Impact: The research uncovered a correlation between defect intensity and the number/intensity of impulses. As defects worsened, the waveform exhibited increased modulation and a higher occurrence of these impulses, aiding in gauging defect severity.

✉ Aydin Azizi, aydin.azizi@brookes.ac.uk; Hamed Mobki, hamedmobki@live.om; Ehsan Shabahang Nia, e.shabahang@gmail.com | [1]Center of Condition Monitoring at Urmia Combined Cycle Power Plant, West Azerbaijan Power Generation Management Company, Urmia 1369, Iran. [2]School of Engineering, Computing and Mathematics, Oxford Brookes University, Wheatley Campus, Oxford OX33 1HX, UK.

- Statistical Analysis: A comprehensive statistical analysis was conducted over 40 days on a continuously running defective electric motor. Over time, certain signal factors stabilized, indicating a consistent pattern as the fault persisted.
- Noise Sensitivity: Investigation into impulse-wise noises highlighted their significant impact on signal factors. However, among these factors, Signal Factor (SF) exhibited the least sensitivity to such noises. Hence, SF emerges as the most robust parameter for effective monitoring procedures.

By detailing these findings, the manuscript emphasizes ultrasound's effectiveness in identifying defects, the evolving nature of signal patterns with fault progression, and the importance of robust parameters for accurate monitoring.

Keywords Condition monitoring · Fault detection · Ultrasound signal · Electro-motor · Fault factor

1 Introduction

Electrical motors and other rotary machines, including pumps, fans, and gearboxes, constitute integral components in various industries such as oil and gas, petrochemicals, and power plants. The monitoring and maintenance of these machines hold paramount importance [1]. Timely detection and rectification of faults in such machinery are crucial to prevent substantial damages. Among the various methods employed for early fault detection, the ultrasound technique has gained substantial attention from both researchers and industry experts in recent times. Scheeren et al. investigated Ultrasonic Wave Transmission in Bearings for Condition Monitoring [2], while the modeling and impact of ultrasonic waves on bearing shells are expounded in [3]. Liu et al. investigated rotational speed of bearing cage using ultrasonic method [4]. Comprehensive review of ultrasonic technology for oil film thickness measurement in lubrication is presented in [5]. Mirmahdi et al. conducted a study on ultrasound wave analysis for defective bearing inner and outer casings [6], and ultrasound signal processing for detecting bearing faults is extensively covered in [7–11].

The ultrasound method operates on the principle of detecting defect frequencies present in the ultrasound signals received from bearings. Owing to the high frequency nature of these signals, early defects such as partial cracks in bearings and the generation of pressure due to rotor imbalance or misalignment can be readily identified [2].

The vibration analysis method is also an efficient method for condition monitoring of rotating machines [12–15], it lacks the rapid fault detection capabilities inherent in ultrasound techniques. Notably, small defects or cracks in bearings do not significantly impact the emitted vibration signal, rendering the ultrasound method an effective means for early defect detection [16–19]. However, this method is not without drawbacks, as the high sensitivity of ultrasound signals to minor shocks unrelated to defects can complicate troubleshooting. The proximity of such defects to the sampling location intensifies the complexity of signal analysis, necessitating consideration not only of signal parameters but also of frequency analysis.

Given the key role of ultrasound in condition monitoring and its increasing application in industrial settings, this article undertakes a comprehensive examination of electro-motor diagnosis using ultrasound waveform analysis. The study explores the influence of signal factors in both faulty and healthy states, incorporating frequency analysis based on envelope analysis and Hilbert transformation. The article underscores that while ultrasound signals exhibit a similar appearance for healthy induction motors, the presence and progression of defects significantly alter the signal waveform. The analysis focuses on machine condition detection based on signal waveform in healthy states, initial fault presence, and advanced fault conditions, drawing insights from experimental-industrial results.

The study explores the changes in waveform shape induced by the presence of defects, impacting crucial signal factors such as peak, crest factor, impulse factor, energy, and more. By presenting results obtained from an electro-motor, the article investigates the rate of changes in these factors with increasing fault severity and identifies the factors with the most significant impact on severity. Additionally, the study examines these factors in healthy conditions, identifying the most effective factor for determining machine condition. Furthermore, the article introduces frequency analysis based on the envelope method with Hilbert transformation for diagnosing healthy and defective modes. The comprehensive analysis also addresses the sensitivity of ultrasound techniques to impulse-wise noise, offering insights through empirical cases. Given the frequent occurrence of such impulses in ultrasound data from healthy machines, the study assesses the impact on signal factors and presents robust factors resilient to these noises.

This paper is organized as follows: the next section provides an overview of utilized mathematical and statistical methods. Section 3 describes the experimental-industrial setup. Section 4 presents the obtained results and relevant discussions. Finally, Sect. 5 presents the concluding remarks of this paper.

2 Mathematical and statistical analysis

2.1 Envelope method

In induction electro-motors operating at a fixed speed, the ultrasound waveform exhibits an oscillatory pattern with nearly uniform maximum amplitudes. This phenomenon will be extensively examined in Sect. 4.1. When a fault arises in either the bearing or electro-motor, this fault induces a distinct waveform, modulated onto the healthy waveform. The primary cause of this modulation lies in the transformed position of the fault, a result of bearing or fault location movement. It is important to note that the ultrasound sensor remains stationary. The modulation amplitude or envelope is a low frequency signal that contains fault information [20, 21]. Envelope is the magnitude of analytical signal that calculated by Hilbert transformation.

Hilbert transform of an ultrasound signal x(t) is $\hat{x}(t)$ which is obtained by convolving x(t) with the signal $\frac{1}{\pi t}$, and can be expressed as [22]:

$$\hat{x}(t) = \frac{1}{\pi t} * x(t) \tag{1}$$

$\hat{x}(t)$ and $x(t)$ are orthogonal signals with phase difference of 90°. The function $\frac{1}{\pi t}$ has a singularity in $t = 0$ and if $x(t)$ is a real signal, then $\hat{x}(t)$ is a real as well. For such case the signal $a(t)$ is an analytical signal [23].

$$a(t) = x(t) + j\hat{x}(t) \tag{2}$$

The envelope of $a(t)$ at time t actually represents its size, and is expressed as $A(t)$:

$$A(t) = \sqrt{[x(t)]^2 + \left[\hat{x}(t)\right]^2} \tag{3}$$

2.2 Condition monitoring factors

As previously explained, the ultrasound signal exhibits a distinctive waveform under healthy conditions. However, when a fault arises in either the electro-motor or bearing, the resultant signal from the fault may become modulated onto the healthy signal. This modulation not only alters the overall shape of the waveform but also induces changes in various signal indicators. The most noteworthy indicator affected by the emergence of a fault is the peak, the level of which undergoes modifications depending upon the type and severity of the defect. Recognizing the key role of statistical analysis in assessing signal factors and their examination in both healthy and defective states to ascertain relevant indicators for monitoring, this section develops the important indicators considered for condition monitoring.

If x_i represents each sample of signal in each time step, where i represents the counter from 1 to N, and N represents the number of the last sample; peak is equal to [24]:

$$peak = \sup |x_i| \tag{4}$$

Also, mean value and RMS of signal is determined as follows [25]:

$$\bar{x} = \frac{\sum_{i=1}^{N} x_i}{N} \tag{5}$$

$$RMS = \sqrt{\frac{1}{N}\sum_{i=1}^{N}\left(x_i - \bar{x}\right)^2} \tag{6}$$

Crest Factor (CF): The Crest Factor, denoted as CF, signifies the ratio of peak to RMS. Given that the presence of a defect often leads to a pronounced increase in peak amplitude compared to RMS, CF emerges as an essential parameter for discerning the machine's condition. This parameter is mathematically expressed as follows [25]:

a. DE side b. NDE side

Fig. 1 an electro-motor under ultrasound condition monitoring, sensor position, and data logger

$$CF = \frac{peak}{RMS} \tag{7}$$

Impulse factor (IF): IF represents the ratio of peak to signal mean-value. The higher the impulse factor in a signal, the greater the intensity of the impulses in a signal [24].

$$IF = N\frac{peak}{\sum_{i=1}^{N} |x_i|} \tag{8}$$

Clearance factor (ClF): Another parameter that exhibits sensitivity to the peak value is the Clearance Factor, denoted as ClF. It can be mathematically expressed as follows [24]:

Fig. 2 data logger SDT 270 and software Ultranalysis Suite 3

Table 1 Specification of studied electro-motor of Sect. 4.1

Mark	SIEMENS
Type	1LA5 207 2AA64-Z 200L
Power	37 kW
Rotor speed	2950 RPM (49.17 Hz)
Type NDE bearing	6212-2Z-C3
Type DE bearing	6212-2Z-C3

$$CIF = \frac{peak}{\left(\frac{1}{N}\sum_{i=1}^{N}\sqrt{|x_i|}\right)^2} \tag{9}$$

Shape factor (SF): As elucidated in subsequent sections, the Shape Factor (SF) emerges as a fundamental factor in the domain of condition monitoring through the ultrasound method. SF denotes the ratio of IF to CF and is formally expressed as follows [24]:

$$SF = N\frac{RMS}{\sum_{i=1}^{N}|x_i|} \tag{10}$$

Kurtosis: This factor is the fourth standardized moment of the signal and Its value is about 3 for Gaussian white noise and also increases with increasing of impulses [25].

$$kurtosis = \frac{N\sum_{i=1}^{N}\left(x_i-\bar{x}\right)^4}{\left[\sum_{i=1}^{N}\left(x_i-\bar{x}\right)^2\right]^2} \tag{11}$$

Kurtosis factor (KF) is also another factor of signal and is directly related to kurtosis as follows [25].

$$KF = \frac{kurtosis}{(RMS)^4} \tag{12}$$

Skewness: It is an indicator that expresses the symmetry of the signal and equals with [25]:

$$skewness = \frac{\frac{1}{N}\sum_{i=1}^{N}\left(x_i-\bar{x}\right)^3}{\left[\frac{1}{N}\sum_{i=1}^{N}\left(x_i-\bar{x}\right)^2\right]^{\frac{3}{2}}} \tag{13}$$

Also, the skewness factor or SkF is expressed as:

$$SkF = \frac{skewness}{(RMS)^3} \tag{14}$$

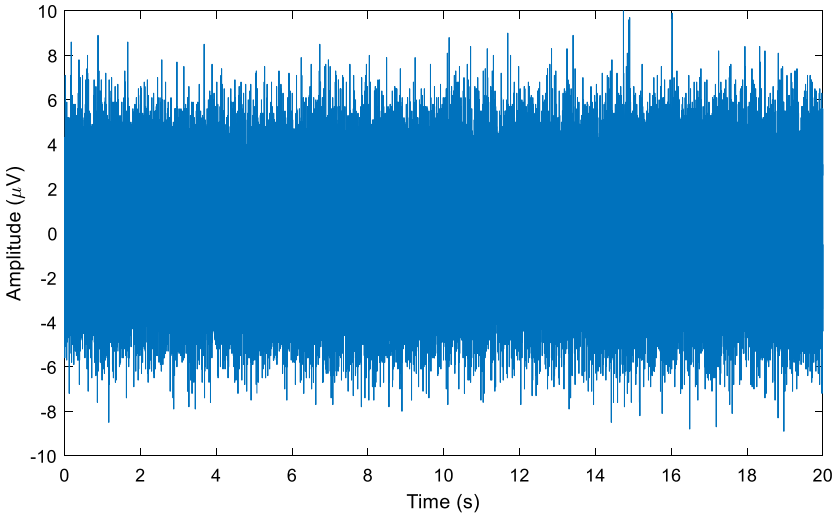

a. waveform of the ultrasonic signal

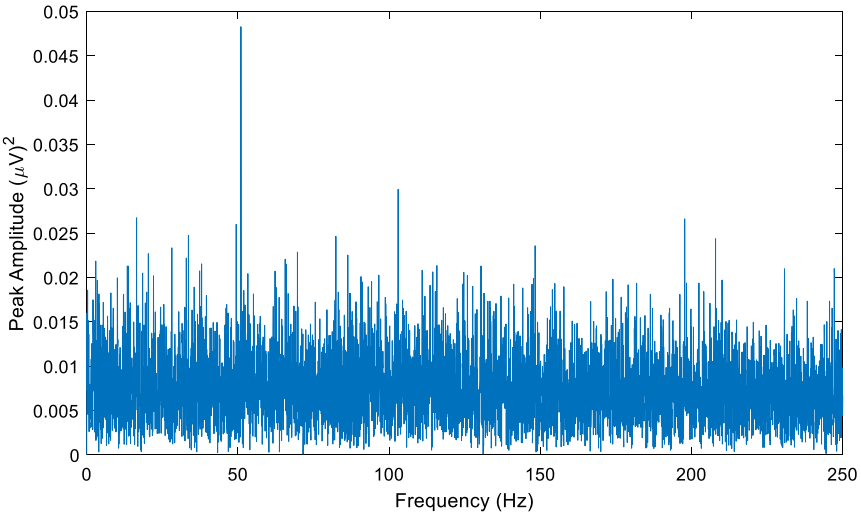

b. envelope diagram of waveform figure 3.a

Fig. 3 Ultrasound signal waveform and its envelope diagram for studied electro-motor of Sect. 4.1. in fault-free condition

3 Experimental-industrial setup

The present study encompasses a detailed analysis of an electro-pump and four distinct types of electro-motors, where specifications and features of each machine will be shown in the subsequent results section. This section focuses on explaining the sampling methodology and the employed data logger. An electro-motor considered for ultrasound data collection is visually depicted in Fig. 1.

For the purpose of diagnosing and monitoring the motor, the ultrasound sensor must be positioned in close proximity to the bearing installation location. On the Non-Drive End (NDE) side of electro-motors, the sensor is ideally situated at a short distance from the cooling fan cover to mitigate ultrasound noise resulting from potential contact between the fan cover screw and the cover. Conversely, as depicted in Fig. 1, on the Drive End (DE) part, the ultrasound sensor is precisely placed at the bearing installation site. Prior to making contact with the sensor-foot, it is necessary to ensure that both the sensor-foot and electro-motor surface are free of any pollution or oil. Therefore, it is required to clean both surfaces thoroughly to avoid any unwanted contamination. The type of sensor is contact RS2T (with curved magnetic foot) with piezoelectric ceramic glued on a mechanical resonant structure that can be affixed over an iron surface. Center frequency (at 20 °C), thermal deviation of the center frequency, measurement band with, and built-in gain are

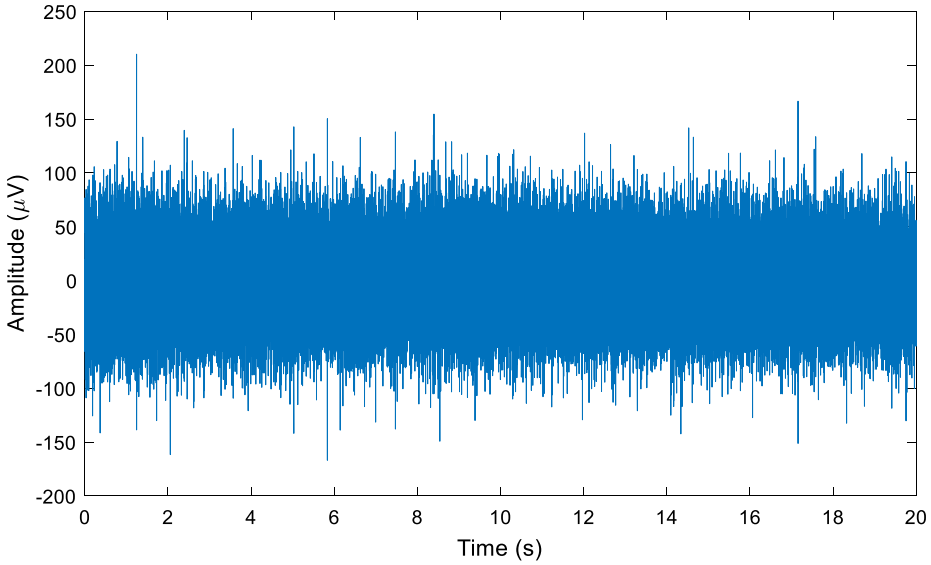

a. waveform of the ultrasonic signal

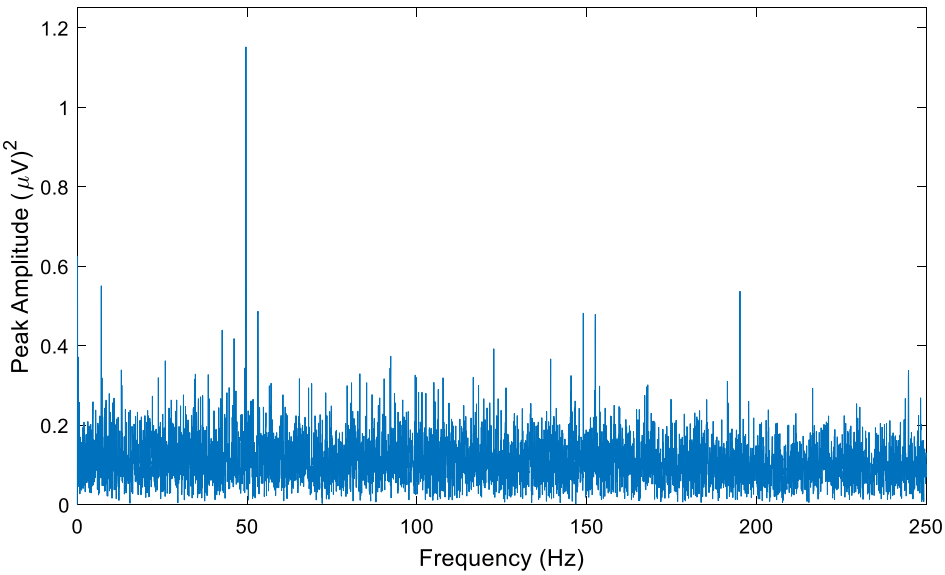

b. envelope diagram of waveform figure 4.a

Fig. 4 Ultrasound signal waveform and its envelope diagram for studied electro-motor of Sect. 4.1. with slight unbalance

37.0 ± 0.5 kHz, −10 Hz/^{0}C, [36.1 kHz, −40.4 kHz], and + 30 dB. Considering the frequency range of electro-motor faults, the sampling frequency is set on 8 kHz sampling rate.

As seen in Fig. 2, the SDT 270 data logger is employed for the recording of ultrasound data. Utilizing the licensed Ultraanalysis Suite 3 software (licensed to WAPGM Company), the ultrasound data is extracted in the form of an Excel file. Subsequently, the data is transferred to MATLAB software for in-depth analysis.

4 Results and discussion

4.1 Examining the signal waveform for different intensities of the fault

The studied electro-motor in this part is a lube oil electro-motor with the specifications illustrated in Table 1.

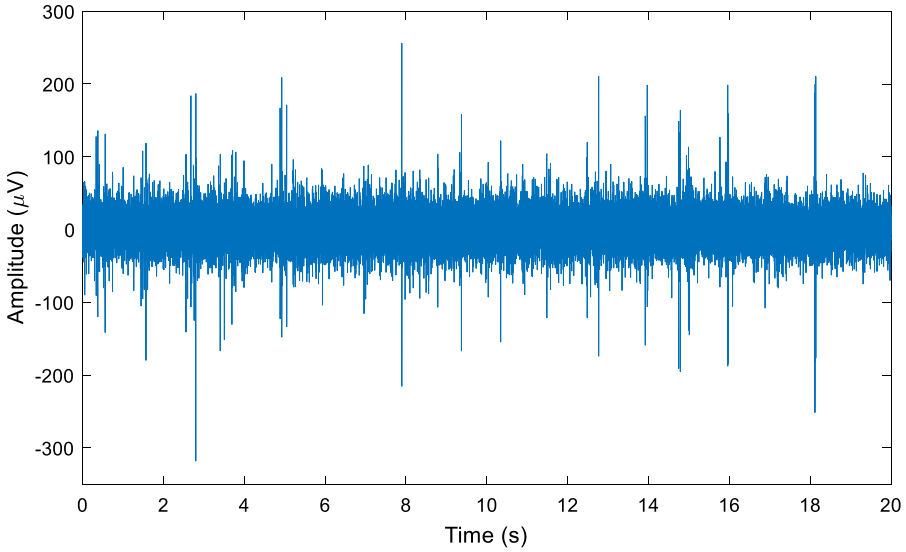

a. waveform of the ultrasonic signal

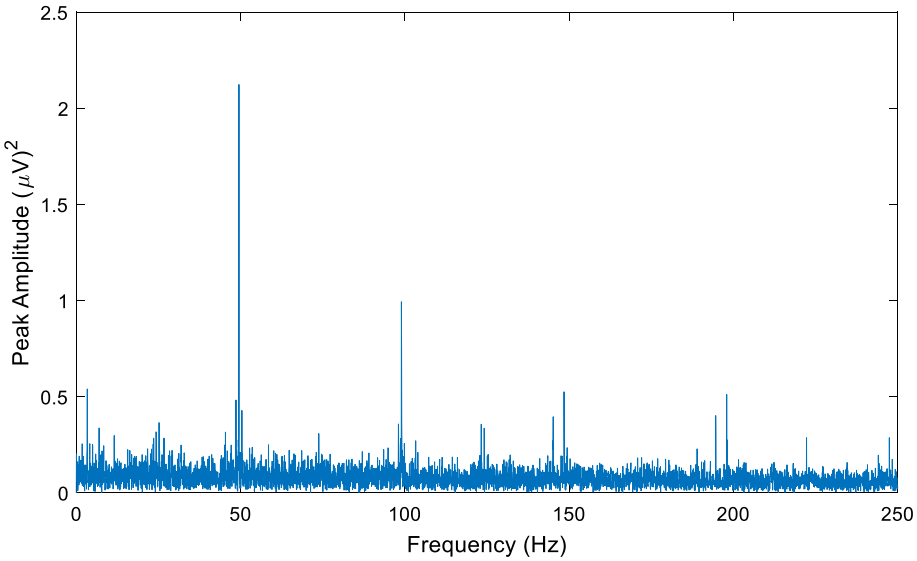

b. envelope diagram of waveform figure 5.a

Fig. 5 Ultrasound signal waveform and its envelope diagram for studied electro-motor of Sect. 4.1. in faulty condition

This section devoted to detailed examination of the ultrasound signal waveform, distinguishing between normal and defective states at various stages. It is crucial to underscore the significance of the electro-pump in question, responsible for lubricating Unit 5 turbo-generator at UCCPP, and operating continuously. Furthermore, it is important to note that the tests conducted are under stationary conditions with a consistent speed.

Additionally, various parameters such as the power consumption of the pump connected to the electric motor remain constant. This includes the viscosity, flow, and discharge of the transmission oil, which exhibit minimal variation. Any substantial change in these parameters during the sampling period could indicate abnormal conditions or a defect in the lubricating system. Importantly, this article focuses exclusively on defects related to the electro-motor, excluding discussions on issues such as transmission fluid specifications.

It is pertinent to highlight that the electric motor has undergone a comprehensive repair process, including the rectification of its unbalance through weighting. The repair process has been effective, resulting in negligible residual

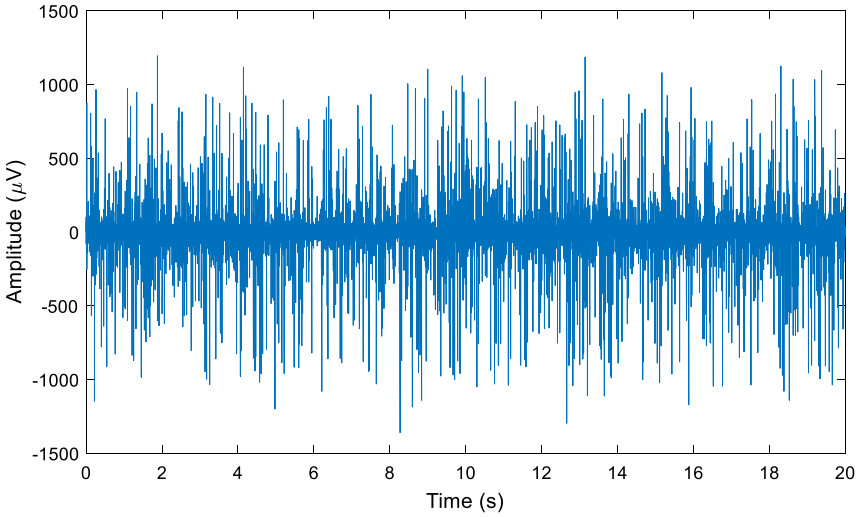

a. waveform of the ultrasonic signal

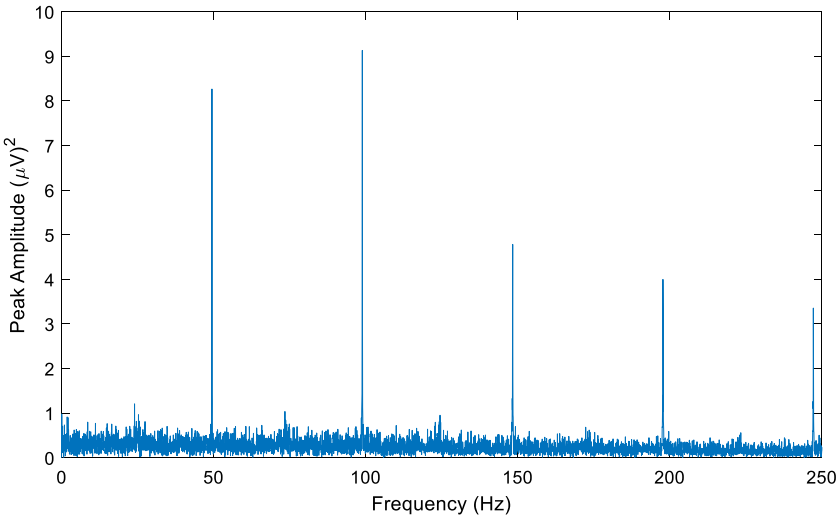

b. envelope diagram of waveform figure 6.a

Fig. 6 Ultrasound signal waveform and its envelope diagram for studied electro-motor of Sect. 4.1. in advanced faulty condition

Table 2 Specification of studied electro-motor of Sect. 4.2

Mark	SIEMENS
Type	1LG4207-2AA64-Z
Power	37 kW
Rotor speed	2950 RPM (49.17 Hz)
Type NDE bearing	6212-2Z-C3
Type DE bearing	6212-2Z-C3

unbalance. Figure 3 depicts the waveform of the ultrasonic signal recorded on November 18, 2021, a few days subsequent to the repair and installation of the electro-motor.

As evident in this figure, the amplitude of the ultrasound signal remains relatively stable throughout the sampling period, devoid of distinct impulses or characteristic waveforms. The corresponding envelope diagram for this mode defines a peak with an approximate amplitude of 0.048 $(\mu V)^2$ at a frequency of 50 Hz, attributable to a slight imbalance in the rotor shaft.

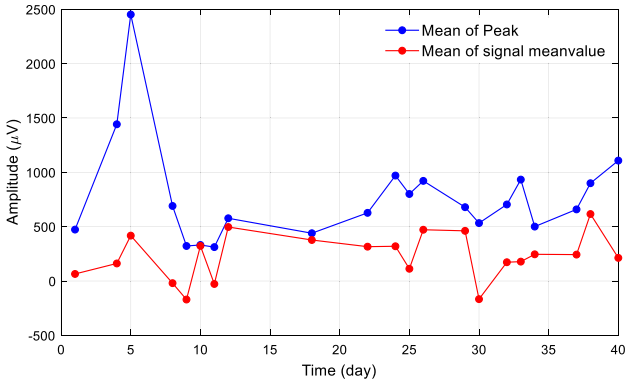

a. NDE bearing

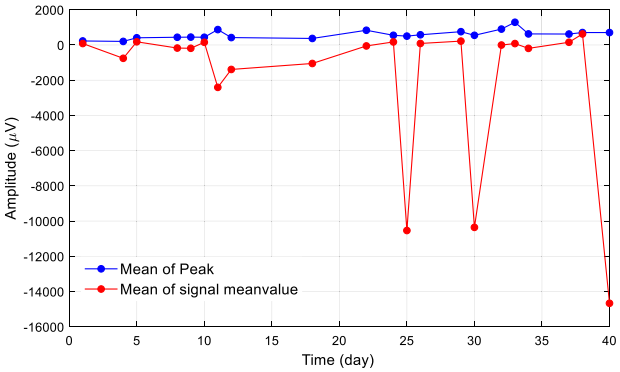

b. DE bearing

Fig. 7 Statistical-average results for peak and mean-value of ultrasound signal of studied electro-motor Sect. 4.2

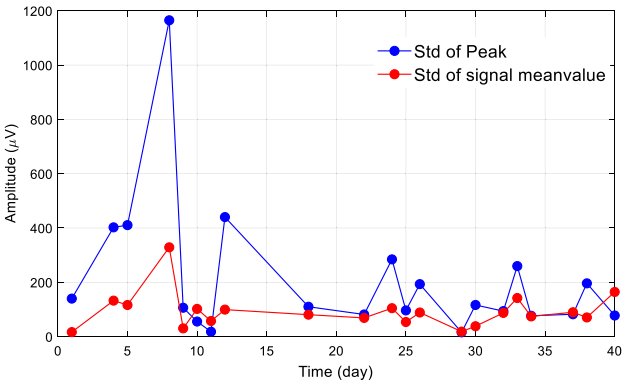

a. NDE bearing

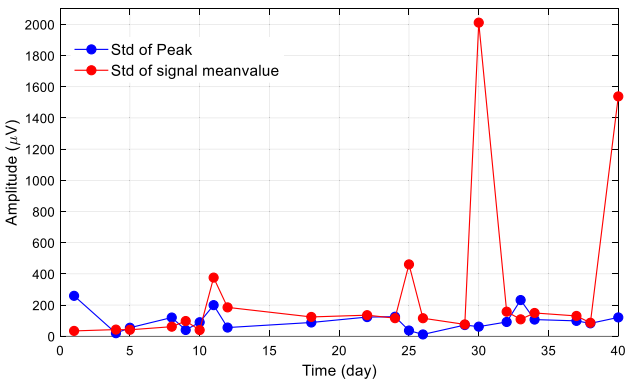

b. DE bearing

Fig. 8 Statistical-std results for peak and mean-value of ultrasound signal of studied electro-motor Sect. 4.2

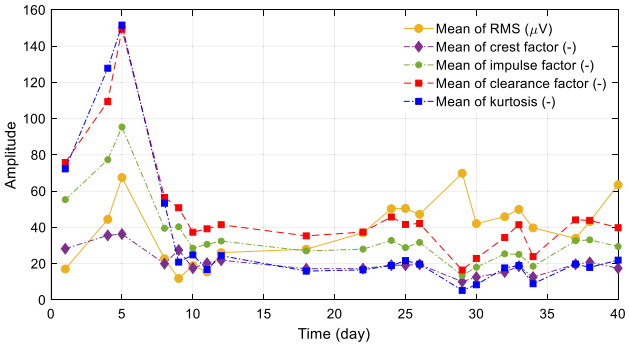

a. NDE bearing

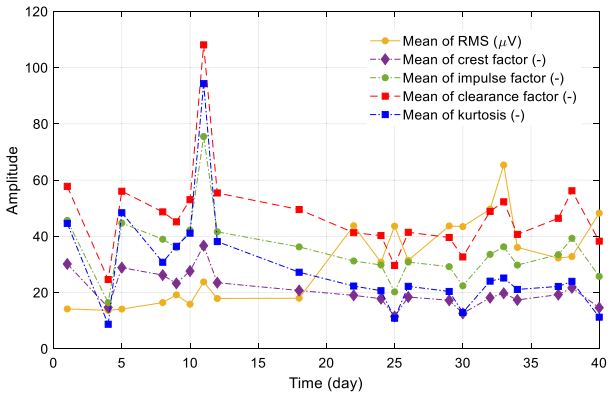

b. DE bearing

Fig. 9 Statistical-average results for RMS, CF, IF, Clf, and kurtosis of ultrasound signal of studied electro-motor Sect. 4.2

Notably, the signal waveform recorded on January 8, 2022, is also presented in Fig. 4. Upon meticulous inspection of this figure, subtle alterations in signal amplitude and the emergence of low-level impulses become apparent compared to Fig. 3. Furthermore, the envelope diagram depicts a peak at 50 Hz with an amplitude of 1.17 $(\mu V)^2$, indicating changes in the ultrasound signal characteristics.

The signal waveform recorded on February 1, 2022, is presented in Fig. 5. As evident in this figure, noteworthy impulses are discernible in the sampling spectrum, accompanied by substantial changes in signal amplitude. The presence of such significant impulses serves as an indicative warning of the severity of the fault, suggesting abnormal conditions in this particular case. The corresponding envelope diagram for this signal is also depicted in Fig. 5b, revealing a distinctive peak with an amplitude of 2.21 $(\mu V)^2$ at a frequency of 50 Hz. Furthermore, noticeable harmonics are evident at frequencies of 100, 150, and 200 Hz.

The signal corresponding to an advanced fault on February 23, 2022, is illustrated in Fig. 6. A noticeable feature in this figure is the significant alteration in the maximum amplitude of the signal. In contrast to Fig. 5, where a few discernible impulses were present in the sampling spectrum, Fig. 6 depicts an increased number of impulses to such an extent that distinguishing two adjacent impulses becomes challenging. In essence, these impulses collectively induce a comprehensive change in the overall waveform shape. The envelope diagram for this state is also explained in Fig. 6b. Significantly, the peaks with substantial amplitude at the frequency of 50 Hz and its harmonics remain clearly distinguishable, despite the heightened complexity of the waveform.

4.2 Statistical investigation of signal factors for defective electro-motor

In this section, a detailed analysis of alterations in the important factors of the ultrasound signal for a faulty electro-motor is accomplished. The specifications of the studied electro-motor are outlined in Table 2. The mentioned electro-motor

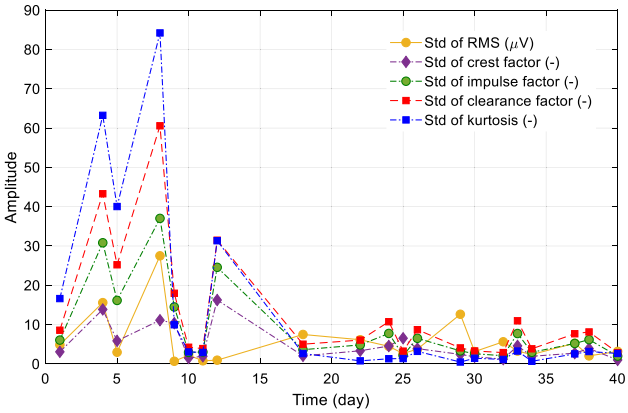

a. NDE bearing

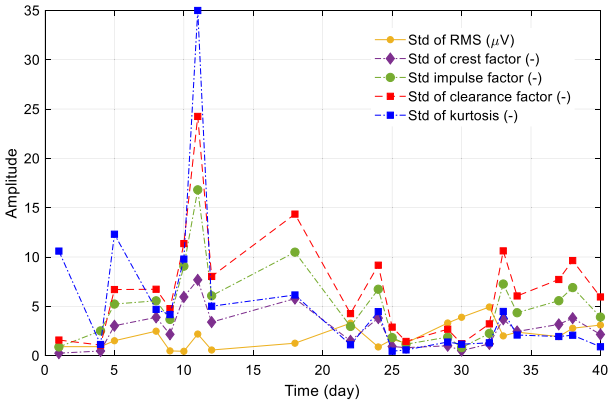

b. DE bearing

Fig. 10 Statistical-std results for RMS, CF, IF, Clf, and kurtosis of ultrasound signal of studied electro-motor Sect. 4.2

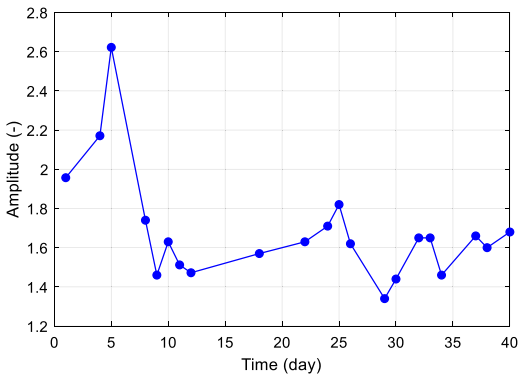

a. NDE bearing

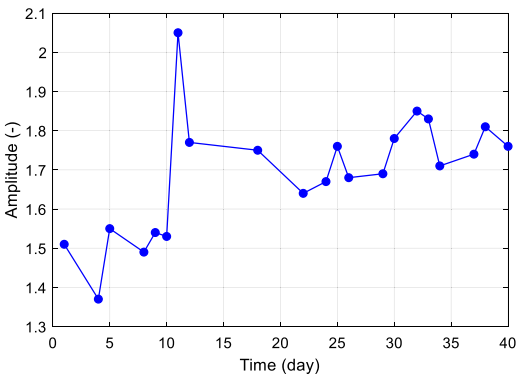

b. DE bearing

Fig. 11 Statistical-average results for SF of ultrasound signal of studied electro-motor Sect. 4.2

underwent previous repairs attributable to rotor shaft unbalance, addressed through weighting. Due to the heightened risk of defect occurrence, continuous monitoring has been in place, revealing a dramatic increase in Shape Factor (SF) and Crest Factor (CF) on 01/08/2022. The last diagnostic test conducted before determining the critical state of the electro-motor was on 01/03/2022, yielding CF and SF values of 4.98 and 1.26, respectively.

Subsequent to 01/08/2022, the electro-motor underwent continuous operation and was monitored for a span of 40 working days. Given the abnormal condition of the electro-motor, multiple consecutive samplings were conducted during each test. The signal factors for each sampling were meticulously determined and are provided in Appendix A,

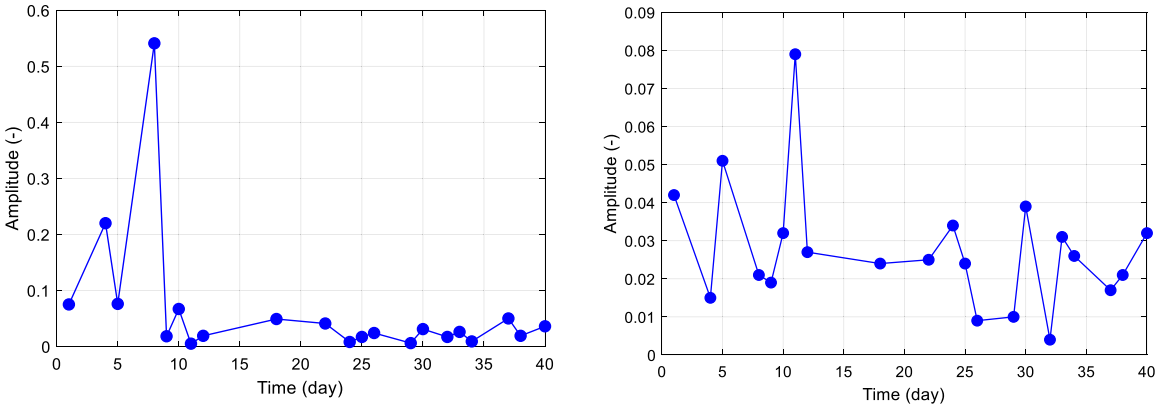

a. NDE bearing b. DE bearing

Fig. 12 Statistical-std results for SF of ultrasound signal of studied electro-motor Sect. 4.2

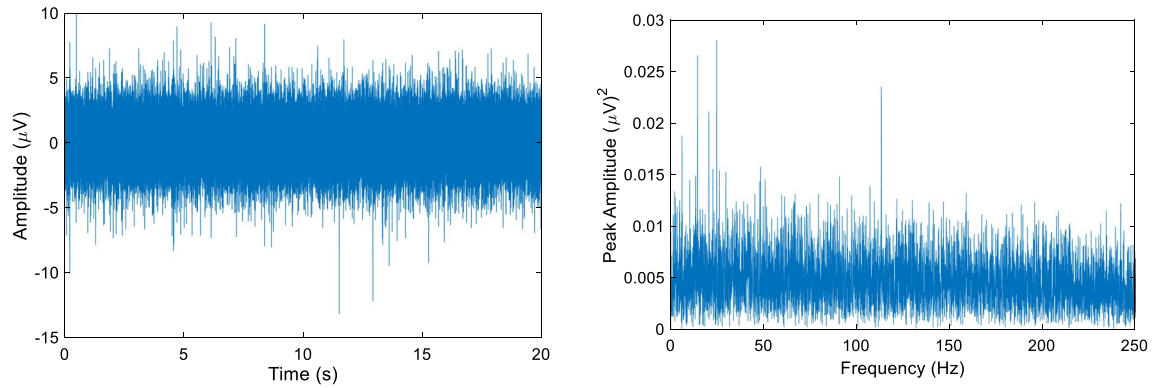

a. waveform of the ultrasonic signal b. envelope diagram of waveform fig 13.a

Fig. 13 Sample No. 1 of Ultrasound signal waveform and its envelope diagram for first case study of Sect. 4.3

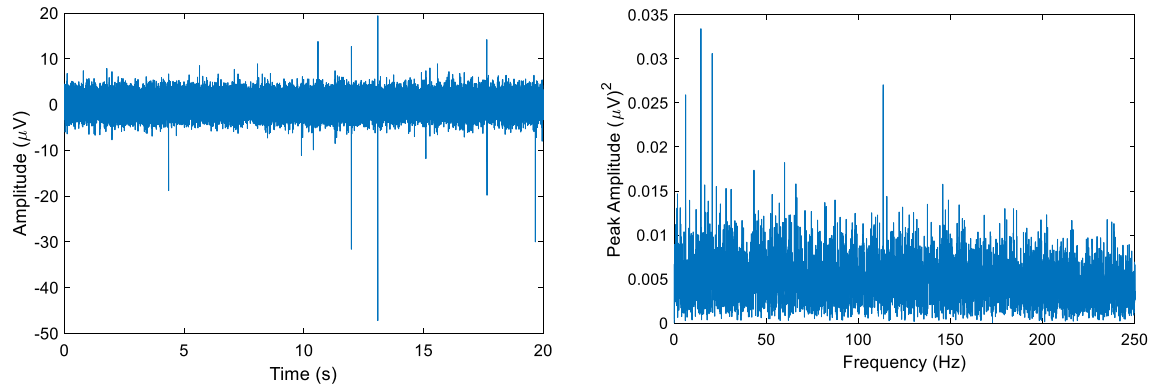

a. waveform of the ultrasonic signal b. envelope diagram of waveform fig ure 14.a

Fig. 14 Sample No. 2 of Ultrasound signal waveform and its envelope diagram for first case study of Sect. 4.3

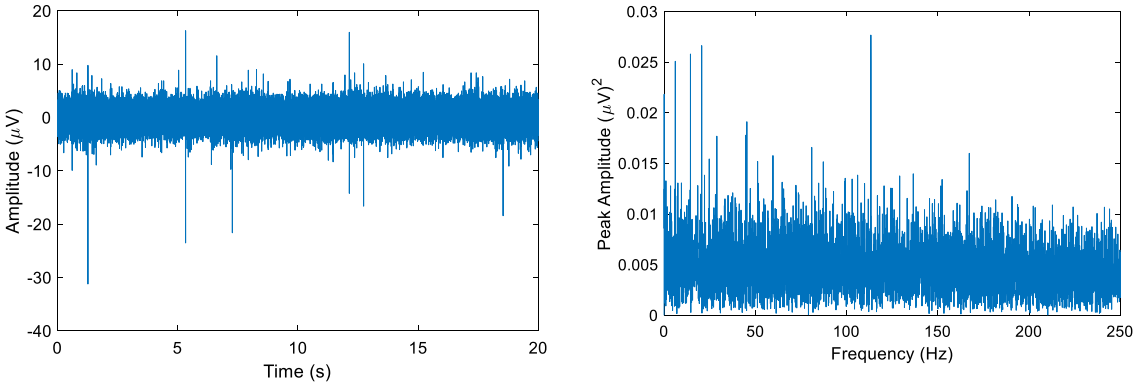

a. waveform of the ultrasonic signal b. envelope diagram of waveform fig ure 15.a

Fig. 15 Sample No. 3 of Ultrasound signal waveform and its envelope diagram for first case study of Sect. 4.3

detailed in Tables 6, 7, 8, and 9. The primary objective of this analysis is to undertake a statistical examination of these factors over the course of 40 days of uninterrupted monitoring.

It is important to note that this electro-motor, assigned to supply of lubricating oil to the turbine and generator of the gas turbine unit 4, remained in operation without interruption throughout the 40-day monitoring period. In all samplings, the gas turbo-generator, generating 110 MW of power, was active. Recognizing that any fluctuations in power generation could affect the operational state of the electro-pump, all samplings were conducted at a consistent power level of 110 MW. Consequently, if there were any changes in the power output of the turbine-generator, ultrasound sampling was omitted.

Given the substantial volume of data, efforts were made to derive the average and standard deviation of the samples for each testing day, facilitating a comprehensive analysis of the continuous monitoring period.

Examining the average of samplings is suitable for checking the trend of factor changes during 40 days, and checking standard deviation (std) may be useful for checking the difference between signal factors on each sampling day. The average and std of signals mean value for NDE and DE bearings are revealed in Figs. 7 and 8.

In this comprehensive analysis spanning 40 days, the examination of key factors within the ultrasound signal for a faulty electro-motor reveals noteworthy patterns. The average peak for both bearings remains relatively consistent, with the NDE bearing exhibiting a higher initial average peak. Conversely, the DE bearing experiences marginal variations in the average peak within the specified timeframe. An exploration of the average signal mean-value unveils a nearly constant rate of change for the NDE bearing, while the DE bearing's average demonstrates significant increases on specific test days. Assessing peak std and mean-value std, a consistent trend emerges. The std value for the NDE bearing's peak, initially significant, diminishes over time, while the DE bearing's peak std maintains relative stability. However, the std of mean-value for the DE bearing exhibits noteworthy values on specific test days. Figures 7b and 8b highlight the challenge in establishing a specific trend for the mean-value of the DE signal. In terms of the peak, discernible decreases in both the average and std are evident over time. Yet, Figs. 7a and 8a underscore significant changes in the average and std of the peak for the NDE bearing in the initial days.

Examining RMS, CF, IF, ClF, and kurtosis, Figs. 9 and 10 illustrate a notable observation. Starting from the 15th day, both the average and std changes for these factors decrease, signifying a transition to a more stable state. However, substantial variations are evident in the early days. Higher std values in these factors imply challenges in precise decision-making due to greater differences among measured samples in tests with multiple samples. This rigorous analysis underscores the evolving nature of the signal over the monitoring period, offering valuable insights into the behavior of the electro-motor under scrutiny. Also, by comparing the CF, IF, ClF, and kurtosis, it is clear that all these factors have almost similar trend. That is, they increase and decrease together. But among these factors, CF has a smaller range of changes compared to other factors.

Another significant parameter to discuss is the SF, which will be shown in the next part, and is considered the chief parameter. Due to the significance of this factor and its lower level compared to other factors, this factor is studied separately. The average and std diagrams for SF during 40 days are displayed in Figs. 11 and 12.

As depicted in these figures, substantial variations are apparent in the early stages following the creation of a defect. However, beyond the 15th day, these changes diminish significantly, attaining a state of stability for this

Table 3 Signal factors for 1st case study of Sect. 4.3

Number of sample (–)	Peak (μV)	Mean (μV)	RMS (μV)	Crest factor (–)	Impulse factor (–)	Shape factor (–)	Clearance factor (–)	Kurtosis (–)	Kurtosis factor $(\mu V)^{-4}$	Skewness (–)	Skewness factor $(\mu V)^{-3}$	energy $(\mu V)^2$
No. 1	13.1	10.55	1.53	8.55	10.87	1.27	12.98	3.58	6487	−11.89	−3305	2.348
No. 2	47.2	12.68	1.53	30.93	39.85	1.29	47.68	14.14	26.067	−448.06	−126.060	2.329
No. 3	31.2	6.96	1.52	20.54	26.40	1.286	31.57	7.84	14.712	−274.96	−78.407	2.308

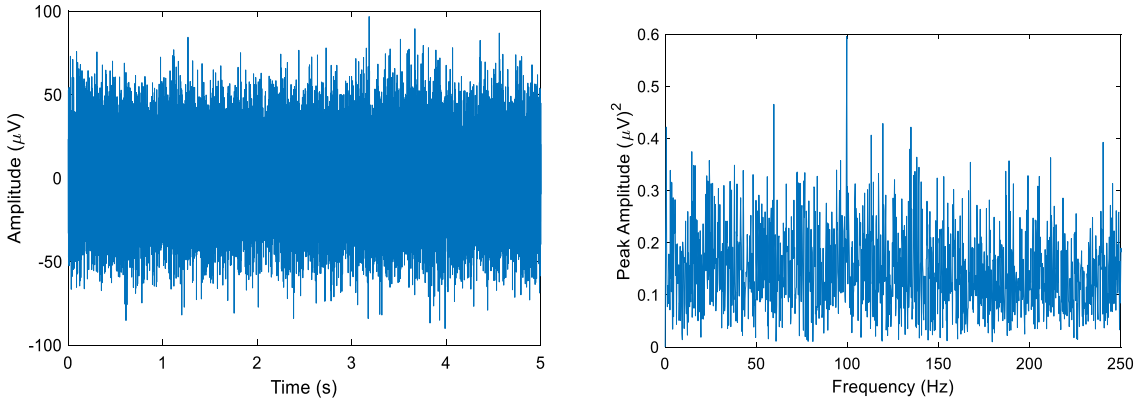

a. waveform of the ultrasonic signal b. envelope diagram of waveform figure 16.a

Fig. 16 Sample No. 1 of Ultrasound signal waveform and its envelope diagram for second case study of Sect. 4.3

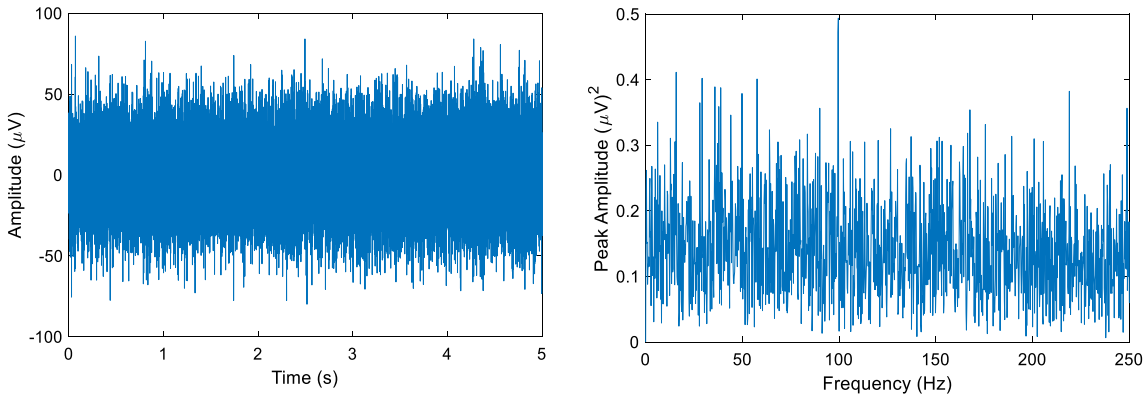

a. waveform of the ultrasonic signal b. envelope diagram of waveform figure 17.a

Fig. 17 Sample No. 2 of Ultrasound signal waveform and its envelope diagram for second case study of Sect. 4.3

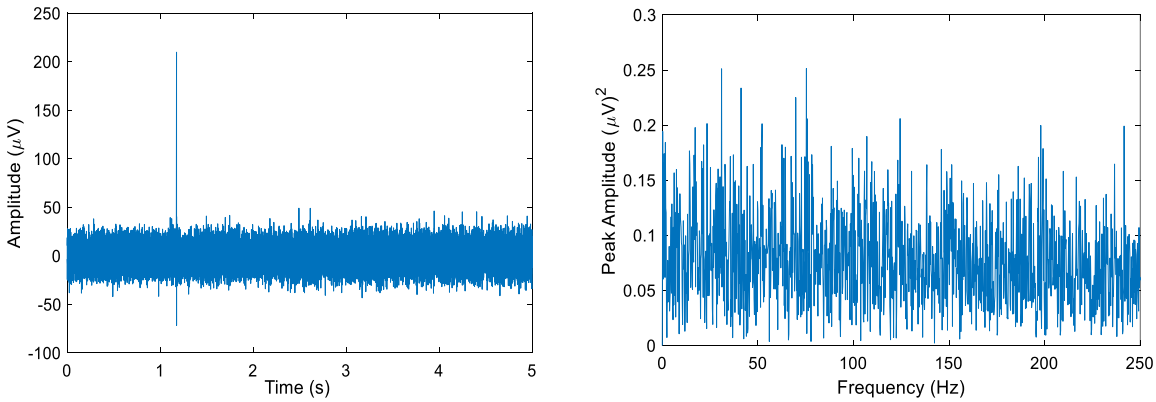

a. waveform of the ultrasonic signal b. envelope diagram of waveform figure 18.a

Fig. 18 Sample No. 3 of Ultrasound signal waveform and its envelope diagram for second case study of Sect. 4.3

Table 4 Signal factors for 2nd case study of Sect. 4.3

Number of sample (–)	Peak (μV)	Mean(μV)	RMS (μV)	Crest factor (–)	Impulse factor (–)	Shape factor (–)	Clearance factor (–)	Kurtosis (–)	Kurtosis factor $(\mu V)^{-4}$	Skewness (–)	Skewness factor $(\mu V)^{-3}$	Energy $(\mu V)^2$
No. 1	96.8	–26.71	22.60	4.28	5.37	1.253	6.33	3.00	0.12	8.80	0.76	510.61
No. 2	85.9	117.56	20.35	4.22	5.30	1.254	6.251	3.04	0.18	6.68	0.793	413.93
No. 3	209.9	134.62	11.30	18.57	23.47	1.264	27.77	7.67	4.70	247.15	171.16	127.75

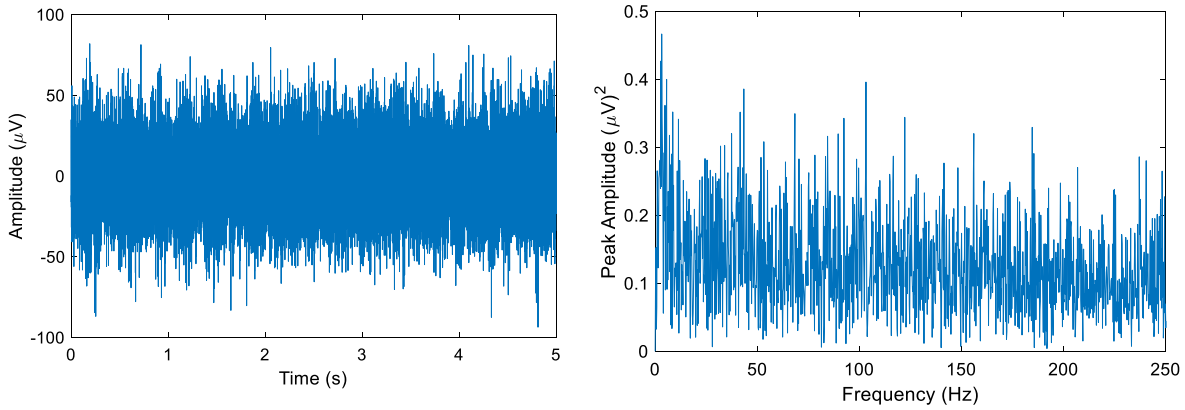

a. waveform of the ultrasonic signal b. envelope diagram of waveform figure 19.a

Fig. 19 Sample No. 1 of Ultrasound signal waveform and its envelope diagram for third case study of Sect. 4.3

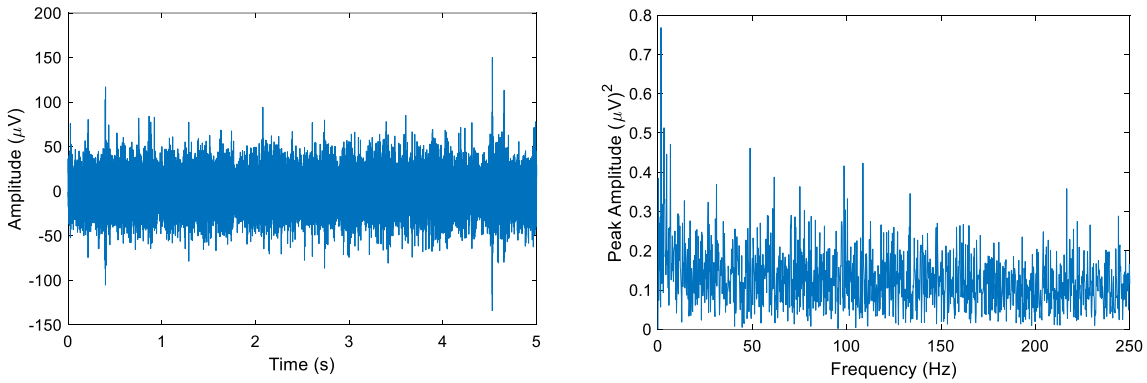

a. waveform of the ultrasonic signal b. envelope diagram of waveform figure 20.a

Fig. 20 Sample No. 2 of Ultrasound signal waveform and its envelope diagram for third case study of Sect. 4.3

specific factor. Notably, the values for this factor consistently surpass 1.3 during the defective state, whereas in normal conditions, as previously highlighted, they typically fluctuate between 1.25 and 1.30. Furthermore, the minimal std associated with this factor underscores its efficacy as a robust indicator for discerning the condition of the bearing or electro-motor.

4.3 Sensitivity of signal factors to the presence of impulse-wise noises

In the context of ultrasound sampling, a notable challenge arises with the occasional presence of impulse-wise noises that are unrelated to underlying defects. These sporadic impulses exert a considerable impact on specific signal factors, complicating the condition monitoring process. Importantly, these impulses do not manifest uniformly across all samples; instead, their occurrence is intermittent in various consecutive samplings. This part of the paper investigates signal factors in the presence of such impulses, utilizing industrial-experimental examples to assess the sensitivity of these factors. The existence of these non-defect-related impulses poses potential challenges to the fault detection process. Furthermore, with the integration of artificial intelligence into condition monitoring and an increasing emphasis on selecting robust factors, this investigation assumes significance. It contributes valuable insights to the robust analysis of fault detection in ultrasound-based condition monitoring.

The first case is related to the NDE bearing of electro-motor SIEMENS (type-1LG42534AA60) with power of 55 kW, rotating speed of 1480 rpm, and 6215-C3 NDE/DE bearing, which has a minor misalignment that does not require repair or replacement of the bearing. Visual representations of the waveform and envelope diagrams for captured signals, derived from three consecutive samples obtained without interruption, are presented in Figs. 13, 14, and 15.

Table 5 Signal factors for third case study of Sect. 4.3

Number of sample (–)	Peak (μV)	Mean(μV)	RMS (μV)	Crest factor(–)	Impulse factor (–)	Shape factor (–)	Clearance factor (–)	Kurtosis (–)	Kurtosis factor $(\mu V)^{-4}$	Skewness (–)	Skew ness factor $(\mu V)^{-3}$	Energy $(\mu V)^2$
No. 1	93.6	−28.25	19.32	4.84	6.16	1.27	7.31	3.34	0.24	10.24	1.42	373.30
No.2	150.1	79.97	18.78	7.99	10.28	1.285	12.275	3.99	0.320	36.399	5.49	352.76

As it is evident from Figs. 14 and 15, impulses with significant amplitude is easily detectable in the waveforms. Such impulses significantly changes the peak levels. Such alteration of peak level changes some factors, which makes misperception in monitoring procedure. For example, IF, CF, and, ClF are directly dependent on peak and its change directly affect these items. The characteristics of the signal factors for these three waveforms are presented in the Table 3.

As it is clear from this table, RMS, SF, and, energy are 4 factors that show very slight sensitivity to the presence of impulse-wise noises. According to the formulas related to the above-mentioned factors, it is clear that a significant change of one or a limited number of x_i cannot cause a significant change in the magnitude of these factors. For RMS and energy, their values in electro-motors or pumps depend on variables such as the electro-motor type, rotation speed, power consumption, etc. Consequently, establishing a specific threshold for the alarm limit of these factors as a universal condition monitoring criterion for all pumps or induction motors proves challenging. However, SF emerges as a valuable tool for assessing the condition of these machines, with a value surpassing 1.3 indicating a critical situation, while a completely healthy electro-motor registers SF between 1.25 and 1.27.

Turning to the second case study, it involves the NDE bearing of a fault-free electro-motor of ABB (type: M2CA-315LA2V1), featuring a power rating of 200 kW, a rotating speed of 2978 rpm, and a NDE/DE bearing of type 6316-C4. Figures 16, 17 and 18 visually represent the outcomes of three consecutive samplings, where Fig. 18 discloses a notable peak or impulse in the signal waveform. The corresponding signal factors are presented in Table 4, revealing that, with the exception of SF, all factors undergo substantial changes in response to the impulse. Unlike Table 3, variations are also observed in RMS and energy.

The last case study is a centrifugal pump with double angular bearing type 7313 B-MP-UA of in coupling side of electro-pump. In this part, it will be shown that SF is also suitable for monitoring of pumps. The results of two consecutive samplings for the corresponding bearing are shown in Figs. 19 and 20, where, calculated factors are listed in Table 5. As it is clear from this table, SF also has a small sensitivity to the existence of impulses. Also, for these two samples, the RMS and energy values do not show significant changes.

5 Conclusion

Considering the significant role of the ultrasound methodology in the condition monitoring of electro-motors and rotating machines, this paper was devoted to comprehensive examination of ultrasound signal characteristics in both healthy and defective electric motors. The initial phase involves a thorough analysis of the ultrasound signal's waveform, inspecting its behavior under varying degrees of defect severity for both healthy and defective states. Subsequently, the frequency spectrum of these states is meticulously extracted using a combination of the envelope method and Hilbert transform.

For the healthy state, it has been shown that the signal waveform has a Gaussian-like behavior, which changes the waveform when a defect is formed and intermittent impulses appear on the waveform. It was also shown that with the intensity of the defect, the intensity of these impulses also growths, and with the continuation of severity, the number of these impulses and their power increases, ultimately resulting in modulations within the waveform.

The subsequent phase involves an extensive statistical analysis of signal factors over a 40-day period on a continuously operational defective electric motor. The finding revealed that with the continuation of the fault and with passing of time, level of some factors reach a steady level. Furthermore, the study explores the ultrasound signal's sensitivity to impulse-wise noises and their consequential impact on signal factors. This exploration underscores that the presence of such impulses significantly influences the magnitude of some signal factors. Excluding, the Shape Factor (SF) demonstrates remarkable robustness, exhibiting the least sensitivity to such noises. Consequently, SF emerges as a robust and reliable parameter, positioning itself as a prime candidate for effective condition monitoring procedures.

Author contributions HM, ESN, and AA all contributed significantly to the creation of this manuscript. HM was involved in conceptualization, methodology, and writing of the original draft. EMN contributed to data curation, formal analysis, and review and editing of the manuscript. AA participated in project administration, supervision, and critically revising the manuscript for important intellectual content. All authors have read and approved the final version of the manuscript, and their collective efforts have contributed substantially to the completion of this work.

Funding This paper is supported with West Azerbaijan Power generation Management Company. Also, all devices and instrument in regard of ultrasound analysis is provided by company of Tadbir Sazan Saramad from budget for development of Steam Power Generation units of Urmia Combined Cycle Power Plant.

Data availability The related data are presented within the manuscript.

Declarations

Competing interests The authors declared no potential competing interests concerning this research, authorship, and publication of this article.

Appendix

See Tables 6, 7, 8, and 9.

Table 6 Obtain ultrasound signal factors of NDE bearing of studied electro-motor Sect. 4.2

Date month/day (number of sample)	Peak (μV)	Mean (μV)	RMS (μV)	Crest factor (–)	Impulse factor (–)	Shape factor (–)	Clearance factor (–)	Kurtosis (–)	Kurtosis factor $(\mu V)^{-4}$	Skewness (–)	Skewness factor $(\mu V)^{-3}$	energy $(\mu V)^2$
1/8 (1)	332.63	55.41	13.19	25.21	47.42	1.88	64.19	62.14	20.52	30.12	13.12	174.04
1/8 (2)	445.13	52.65	16.18	27.50	55.21	2.00	76.39	78.49	78.49	11.45	−119.98	261.88
1/8 (3)	477.63	62.31	14.68	32.52	62.13	1.91	84.82	55.78	12	83.29	26.3	215.60
1/8 (4)	667	88.93	24.10	27.70	56.53	2.04	77.79	92.65	2.76	−635	−45.35	580.90
1/11 (1)	1211	294.33	33.69	35.94	72.2	2.00	101.22	82.36	0.64	−393	−10.27	1135
1/11 (2)	1219	208.73	37.95	32.13	66.99	2.09	94.13	98.96	0.48	237.68	4.35	1440
1/11 (3)	1951	329.02	35.07	55.62	110.35	1.98	149.10	188.54	1.25	1129	26.18	1230
1/11 (4)	1410	157.19	45.6	30.91	66.16	2.14	94.12	109.28	0.25	−92.25	−0.97	2080
1/11 (5)	2179	212.02	41.00	53.14	117.12	2.20	164.83	191.45	0.68	−1107	−16.05	1681
1/11 (6)	1222	−47.29	66.12	18.48	40.40	2.19	57.96	72.21	0.04	−720.90	−2.49	4372
1/11 (7)	1295	−7.12	69.73	18.58	38.79	2.09	55.70	57.29	0.02	−414.83	−1.22	4863
1/11 (8)	1046	144.94	26.19	39.92	106.82	2.68	158.48	222.42	4.72	−1069	−59.49	686.11
1/12 (1)	2576	481.88	63.55	40.54	107	2.64	170.57	143.49	0.09	−852.14	−3.32	4038
1/12 (2)	1847	368.83	66.19	27.90	74.25	2.66	117.27	122.07	0.064	−274.69	−0.95	4382
1/12 (3)	2236	253.98	68.40	32.69	81.84	2.50	126.78	107.98	0.05	−317	−0.99	4679
1/12 (4)	2833	420.86	67.75	41.81	109.25	2.61	168.1	180.73	0.09	−116.22	−0.37	4590
1/12 (5)	2770	562.06	71.63	38.67	104.64	2.70	163.60	203.79	0.08	−1757	−4.79	5130
1/15 (1)	93.25	−188.25	7.31	12.74	18.27	1.43	22.71	11.90	41.52	−20.79	−53.1	53.53
1/15 (2)	84.18	−231.82	7.69	10.94	15.70	1.43	19.52	11.28	32.24	−106.84	−234.96	59.13
1/15 (3)	271.38	−133.1	13.06	20.78	32.87	1.58	42.82	21.31	7.32	129.42	58.08	170.61
1/15 (4)	233.94	−107.66	13.97	16.75	26.12	1.56	33.89	18.43	4.85	−26.95	−9.90	195.03
1/16 (1)	392.88	−187.01	10.76	36.52	52.68	1.44	65.91	31.07	23.21	515.60	414.25	115.71
1/16 (2)	469.44	−163.63	11.65	40.29	58.51	1.45	73.53	32.42	17.58	466.85	295.04	135.79
1/16 (3)	221.13	−160.80	12.17	18.18	26.82	1.48	34.00	13.83	6.31	235.37	130.69	148.03
1/16 (4)	236.25	−129.99	12.52	18.88	27.96	1.48	35.54	13.48	5.50	103.83	52.96	156.65
1/16 (5)	291.50	−210.81	12.00	24.28	35.67	1.47	45.14	13.44	6.47	−181.95	−105.13	144.16
1/17 (1)	325.32	461.36	19.00	17.11	29.07	1.70	38.66	28.88	2.21	39.89	5.81	361.28
1/17 (2)	272.55	365.33	15.93	17.11	26.26	1.54	33.57	21.93	3.40	−62.23	−15.38	253.89
1/17 (3)	321.17	320.59	17.62	18.23	28.88	1.58	37.33	25.27	2.62	114.79	20.98	310.51
1/17 (4)	315.24	283.14	20.27	15.55	25.42	1.63	33.45	21.71	1.285	−81.54	−9.78	411.04
1/17 (5)	423.36	184.87	21.60	19.60	32.90	1.68	43.74	26.40	1.21	−89.17	−8.85	466.60
1/18 (1)	329.38	57.96	14.33	22.99	34.97	1.52	44.79	20.61	4.89	185.850	63.07	205.27
1/18 (2)	286.82	−67.51	15.55	18.44	27.91	1.51	35.74	13.94	2.38	−103.07	−27.41	241.80
1/18 (3)	314.94	−47.66	15.66	20.11	30.27	1.51	38.55	17.45	2.90	−70.42	−18.32	245.35
1/18 (4)	316.63	−51.84	16.19	19.56	29.51	1.51	37.77	15.23	2.22	107.60	25.38	261.96

Table 6 (continued)

Date month/day (number of sample)	Peak (μV)	Mean (μV)	RMS (μV)	Crest factor (–)	Impulse factor (–)	Shape factor (–)	Clearance factor (–)	Kurtosis (–)	Kurtosis factor $(\mu V)^{-4}$	Skewness (–)	Skewness factor $(\mu V)^{-3}$	energy $(\mu V)^2$
1/19 (1)	333.82	666.87	25.15	13.27	19.55	1.47	24.99	10.59	0.265	−86.47	−5.44	632.41
1/19 (2)	273.74	468.93	25.27	10.83	15.80	1.46	20.12	8.91	0.22	−97.97	−6.07	638.32
1/19 (3)	1350	457.36	26.74	50.50	75.72	1.50	96.89	80.41	1.57	1202	69.20	715.02
1/19 (4)	485.61	406.81	25.93	18.73	27.24	1.45	34.61	10.38	0.23	8.57	0.49	672.18
1/19 (5)	442.73	483.38	27.37	16.18	23.99	1.48	30.74	11.62	0.21	125.33	6.11	748.94
1/25 (1)	372.17	441.09	22.23	16.74	26.06	1.56	33.88	15.55	0.64	139.24	12.68	494.10
1/25 (2)	311.09	405.49	22.40	13.89	21.27	1.53	27.56	13.23	0.53	25.74	2.29	501.77
1/25 (3)	410.90	449.11	22.56	18.22	27.72	1.52	35.80	13.61	0.53	65.35	5.69	508.84
1/25 (4)	527.12	259.02	27.54	19.14	30.43	1.59	39.90	19.44	0.34	−24.14	−1.16	758.58
1/25 (5)	576.73	331.53	32.03	18.00	29.55	1.64	39.46	17.62	0.17	108.57	3.30	1026
1/29 (1)	645.51	229.13	41.04	15.73	26.35	1.68	35.76	17.92	0.062	9.58	0.139	1684
1/29 (2)	654.40	266.82	45.60	14.35	23.82	1.66	32.23	16.31	0.04	−66.50	−0.70	2079
1/29 (3)	516.84	331.02	31.42	16.45	26.56	1.61	35.33	16.12	0.17	−13.78	−0.44	986.92
1/29 (4)	734.45	403.90	31.95	22.99	36.37	1.58	47.94	16.46	0.16	77.66	2.38	1020
1/29 (5)	584.64	348.40	34.86	16.77	26.97	1.61	35.87	15.99	0.11	−5.72	−0.135	1215
1/31 (1)	820.82	447.95	43.17	19.01	32.47	1.71	44.95	19.94	0.06	14.04	0.17	1863
1/31 (2)	808.17	338.14	48.98	16.50	28.30	1.72	39.52	18.17	0.03	−31.02	−0.26	2399
1/31 (3)	763.90	161.32	51.86	14.73	25.40	1.72	35.67	17.42	0.02	−116.50	−0.84	2690
1/31 (4)	1007	356.41	53.04	18.99	32.33	1.70	44.95	18.68	0.02	46.56	0.31	2813
1/31 (5)	1451	294.39	54.48	26.64	45.63	1.71	63.61	20.65	0.02	−144.02	−0.89	2968
2/1 (1)	745.01	166.18	49.13	15.16	27.62	1.82	39.66	21.95	0.038	−100.97	−0.852	2414
2/1 (2)	759.57	85.64	48.54	28.78	28.79	1.84	41.94	22.41	0.04	−228.49	−2.00	2356
2/1 (3)	752.89	50.61	49.81	15.11	27.14	1.80	38.87	19.66	0.03	−206.62	−1.67	2481
2/1 (4)	945.01	147.79	54.36	17.38	31.89	1.83	46.12	22.60	0.03	−214.77	−1.33	2955
2/2 (1)	965.89	616.36	41.96	23.02	37.02	1.61	48.84	21.87	0.07	−15.92	−0.22	1761
2/2 (2)	791.57	486.44	44.64	17.73	28.28	1.59	37.29	16.63	0.04	27.95	0.31	1993
2/2 (3)	881.50	442.31	49.16	17.93	29.36	1.64	39.16	19.77	0.03	−91.73	−0.77	2417
2/2 (4)	1230	428.56	50.91	24.17	39.88	1.65	53.30	23.81	0.035	−149.92	−1.14	2592
2/2 (5)	737.81	384.21	49.36	14.95	24.13	1.61	32.09	16.57	0.028	−58.13	−0.48	2437
2/5 (1)	702.04	479.58	51.56	13.61	18.36	1.34	22.46	5.89	0.008	4.45	0.032	2659
2/5 (2)	676.54	463.31	71.43	9.47	12.73	1.34	15.60	5.32	0.002	14.32	0.04	5109
2/5 (3)	668.63	467.40	78.18	8.55	11.41	1.33	13.91	5.00	0.001	−13.62	−0.028	6111
2/5 (4)	669.62	436.04	78.33	8.55	11.40	1.33	13.91	4.79	0.001	−2.86	−0.01	6136
2/6 (1)	406.51	−113.98	38.34	10.60	14.99	1.41	18.90	6.91	0.032	−6.31	−0.11	1470
2/6 (2)	511.13	−172.03	41.52	12.31	17.54	1.43	22.23	7.85	0.026	−3.21	−0.045	1724

Table 6 (continued)

Date month/day (number of sample)	Peak (μV)	Mean (μV)	RMS (μV)	Crest factor (–)	Impulse factor (–)	Shape factor (–)	Clearance factor (–)	Kurtosis (–)	Kurtosis factor $(\mu V)^{-4}$	Skewness (–)	Skewness factor $(\mu V)^{-3}$	energy $(\mu V)^2$
2/6 (3)	525.30	−176.29	42.54	12.35	18.29	1.48	23.58	10.33	0.032	25.11	0.326	1810
2/6 (4)	688.57	−205.22	45.94	14.99	21.27	1.42	26.84	8.30	0.019	−30.48	−0.314	2110
2/8 (1)	565.46	247.38	36.31	15.57	25.66	1.65	34.53	18.82	0.108	0.39	0.008	1319
2/8 (2)	742.36	262.19	45.90	16.17	26.90	1.66	36.56	17.87	0.040	41.44	0.428	2107
2/8 (3)	783.07	68.44	47.79	16.38	26.94	1.64	36.35	16.81	0.032	−19.92	−0.182	2284
2/8 (4)	778.53	96.52	50.65	15.37	25.76	1.68	35.06	18.56	0.028	56.87	0.438	2564
2/8 (5)	651.64	189.16	48.87	13.34	21.86	1.64	29.47	16.16	0.028	31.47	0.275	2388
2/9 (1)	750.46	460.94	44.48	16.87	27.81	1.65	37.50	18.80	0.048	46.26	0.53	1978
2/9 (2)	734.05	178.66	46.34	15.84	25.85	1.63	34.65	17.07	0.037	−93.68	−0.941	2148
2/9 (3)	1377	32.88	52.03	26.47	44.94	1.70	61.16	25.91	0.035	−106.40	−0.755	2707
2/9 (4)	1209	45.67	51.78	23.36	38.39	1.64	51.78	19.57	0.027	−195.84	−1.41	2681
2/9 (5)	850.47	185.71	53.12	16.01	25.97	1.62	34.76	16.23	0.02	−42.61	−0.284	2821
2/9 (6)	707.96	137.64	51.71	13.69	22.69	1.66	30.62	17.08	0.024	−46.16	−0.33	2674
2/9 (7)	902.65	206.49	50.03	18.04	29.57	1.64	39.67	17.95	0.029	−128.15	−1.02	2504
2/10 (1)	486.80	334.37	37.73	12.90	18.98	1.47	24.45	9.14	0.045	33.40	0.62	1424
2/10 (2)	531.47	269.93	39.95	13.30	19.61	1.47	25.37	8.55	0.034	43.72	0.69	1596
2/10 (3)	441.14	192.66	37.27	11.84	17.37	1.46	22.30	9.14	0.047	−10.68	−0.206	1389
2/10 (4)	616.46	282.94	40.62	15.17	22.37	1.47	28.79	9.71	0.036	9.84	0.147	1650
2/10 (5)	427.11	148.19	43.15	9.90	14.37	1.45	18.42	7.96	0.0229	−45.43	−0.566	1862
2/13 (1)	648.67	296.28	27.15	23.90	40.52	1.70	55.64	22.00	0.405	36.69	1.83	736.88
2/13 (2)	632.07	248.32	27.98	22.59	37.61	1.66	50.98	22.28	0.364	−81.26	−3.71	782.61
2/13 (3)	520.40	144.57	30.65	16.98	27.05	1.59	35.81	16.45	0.187	−61.78	−2.51	939.34
2/13 (4)	618.63	391.93	35.73	17.31	27.80	1.61	36.92	16.53	0.101	−25.94	−0.57	1277
2/13 (5)	686.22	188.49	39.45	17.39	28.82	1.66	38.76	20.22	0.083	118.39	1.93	1557
2/13 (6)	766.47	283.13	39.56	19.38	31.59	1.63	42.25	18.98	0.078	36.87	0.596	1565
2/14 (1)	748.68	694.60	40.40	18.53	30.22	1.63	40.32	19.61	0.074	41.97	0.637	1632
2/14 (2)	732.08	625.80	40.87	17.91	28.52	1.59	37.72	17.16	0.0615	−5.822	−0.085	1671
2/14 (3)	791.37	566.57	43.84	18.05	28.60	1.58	37.95	14.74	0.04	−27.73	−0.329	1922
2/14 (4)	1256	695.60	44.46	28.25	44.99	1.59	59.53	23.29	0.06	2.86	0.0325	1977
2/14 (5)	923.60	519.06	44.35	20.83	33.34	1.60	44.13	17.52	0.045	−97.87	−1.122	1967
2/14 (6)	946.52	595.33	45.27	20.91	33.03	1.58	43.82	15.25	0.0363	−56.028	−0.604	2049
2/16 (1)	1084	102.36	63.86	16.97	29.03	1.71	39.60	22.16	0.0133	−246.23	−0.945	4079
2/16 (2)	1050	451.54	60.96	17.22	28.26	1.64	38.00	18.38	0.0133	−88.70	−0.392	3716
2/16 (3)	1014	260.96	58.94	17.21	28.14	1.64	37.59	19.59	0.0162	−224.30	−1.095	3474

Table 6 (continued)

Date month/day (number of sample)	Peak (μV)	Mean (μV)	RMS (μV)	Crest factor (–)	Impulse factor (–)	Shape factor (–)	Clearance factor (–)	Kurtosis (–)	Kurtosis factor $(\mu V)^{-4}$	Skewness (–)	Skewness factor $(\mu V)^{-3}$	energy $(\mu V)^2$
2/16 (4)	1227	332.39	63.41	19.34	33.18	1.72	45.08	25.74	0.0159	53.48	0.21	4021
2/16 (5)	1165	117.46	65.92	17.67	30.01	1.70	40.78	22.22	0.012	−327.73	−1.144	4345
2/16 (6)	1109	12.19	67.67	16.39	27.95	1.70	37.96	23.54	0.0112	−332.71	−1.07	4579

Table 7 Obtained ultrasound signal factors of DE bearing of studied electro-motor Sect. 4.2

Date month/day—(number of sample)	Peak (μV)	Mean (μV)	RMS (μV)	Crest factor (–)	Impulse factor (–)	Shape factor (–)	Clearance factor (–)	Kurtosis (–)	Kurtosis factor $(\mu V)^{-4}$	Skewness (–)	Skewness factor $(\mu V)^{-3}$	energy $(\mu V)^2$
1/8—1	411.07	106.67	13.54	30.35	45.02	1.48	56.66	37.11	11.03	−660.12	−265.74	183.42
1/8—2	444.69	58.49	14.82	30.00	46.27	1.54	58.89	52.10	10.79	−28.74	−8.82	219.75
1/11—1	180.43	−709.35	12.65	14.26	19.31	1.35	23.52	7.52	2.93	−124.90	−61.66	160.09
1/11—2	206.34	−771.22	13.99	14.75	20.21	1.37	24.74	8.90	2.32	−129.21	−47.20	195.68
1/11—3	218.52	−790.74	14.38	15.20	20.94	1.38	25.66	9.77	2.29	−270.47	−91.04	206.65
1/12 -1	318.88	213.90	12.29	25.94	38.51	1.48	47.78	32.27	14.14	−28.77	−15.49	151.07
1/12—2	418.38	154.88	12.77	32.77	49.70	1.52	61.67	56.97	21.44	−161.54	−77.62	163.00
1/12—3	440.38	139.73	14.75	29.86	47.13	1.58	59.36	52.11	11.01	−561.94	−175.15	217.53
1/12—4	472.69	158.44	15.70	30.10	48.59	1.61	61.59	61.55	10.12	−431.99	−111.56	246.60
1/12—5	388.57	234.31	15.15	25.64	39.69	1.55	49.87	39.11	7.42	204.71	58.82	229.65
1/15—1	497.57	−241.04	17.45	28.51	42.57	1.49	53.12	36.30	3.91	−159.95	−30.10	304.52
1/15—2	462.38	−190.57	17.31	26.71	39.00	1.46	48.44	29.43	3.28	7.94	1.53	300.00
1/15 -3	529.20	−175.29	18.23	29.02	43.21	1.49	53.95	32.27	2.92	219.22	36.16	332.47
1/15—4	262.82	−93.64	12.77	20.58	31.11	1.51	39.29	25.17	9.46	−70.07	−33.63	163.14
1/16—1	498.00	−305.14	18.79	26.51	41.18	1.55	51.90	39.23	3.15	−118.67	−17.90	352.88
1/16—2	456.94	−199.19	19.08	23.94	37.28	1.56	46.91	37.45	2.82	213.56	30.72	364.21
1/16—3	386.57	−242.22	18.69	20.68	31.14	1.51	38.86	29.29	2.40	−327.17	−50.07	349.49
1/16—4	440.69	−47.77	19.68	22.40	34.80	1.55	43.75	36.90	2.46	116.35	15.27	387.22
1/16 -5	449.26	−148.80	19.69	22.82	35.36	1.55	44.38	39.48	2.63	−294.07	−38.53	387.67
1/17—1	518.38	199.60	15.28	33.93	51.48	1.52	64.53	40.63	7.45	199.14	55.82	233.47
1/17—2	321.44	111.19	15.94	20.16	31.20	1.55	39.32	37.98	5.88	275.23	67.93	254.15
1/17—3	497.76	130.84	16.34	30.46	47.46	1.56	59.82	54.59	7.66	−94.21	−21.60	266.98
1/17—4	415.13	170.17	15.96	26.00	38.74	1.49	48.46	31.32	4.82	265.28	65.19	254.88
1/18 -1	892.26	−2167	22.29	40.03	82.60	2.06	117.38	109.33	4.43	−2903	−262.20	496.77
1/18—2	936.51	−2737	26.09	35.89	77.04	2.15	112.02	105.17	2.27	−2325	−130.91	680.74
1/18—3	1097	−2744	26.59	41.25	88.12	2.14	128.38	129.99	2.60	−2144	−114.10	706.84
1/18 -4	624.70	−2016	21.32	29.30	57.41	1.96	80.86	52.92	2.56	−2308	−238.19	454.49
1/18—5	1047	−2020	22.26	47.04	94.74	2.01	133.84	120.20	4.89	−1495	−135.42	495.70
1/18—6	644.51	−2759	24.18	26.65	53.08	1.99	76.11	48.24	1.41	−2928	−207.05	584.84
1/19 -1	368.63	−1473	18.31	20.14	35.78	1.78	47.80	33.33	2.97	−2707	−441.20	335.17
1/19—2	469.44	−1195	17.25	27.21	47.37	1.74	62.65	40.01	4.52	−2119	−412.76	297.60
1/19—3	424.13	−1239	17.32	24.49	43.38	1.77	57.67	40.67	4.52	−2817	−542.40	299.87
1/19 -4	479.19	−1353	18.46	25.96	46.89	1.81	62.90	44.14	3.80	−2438	−387.79	340.66
1/19—5	358/69	−1390	18.17	19.74	34.60	1.75	46.12	32.54	2.99	−2615	−436.21	330.02
1/25—1	343.44	−963.70	17.81	19.29	33.44	1.73	45.59	24.78	2.47	−1109	−196.39	317.02

Table 7 (continued)

Date month/day—(number of sample)	Peak (μV)	Mean (μV)	RMS (μV)	Crest factor (–)	Impulse factor (–)	Shape factor (–)	Clearance factor (–)	Kurtosis (–)	Kurtosis factor $(\mu V)^{-4}$	Skewness (–)	Skewness factor $(\mu V)^{-3}$	energy $(\mu V)^2$
1/25—2	378.69	−1103	19.73	19.20	33.86	1.76	46.66	25.75	1.70	−1348	−175.55	389.14
1/25—3	273.44	−936.81	17.69	15.45	26.54	1.72	36.06	22.22	2.27	−1378	−248.74	313.04
1/25—4	484.82	−1201	16.73	28.97	51.15	1.77	69.84	36.19	4.61	−2270	−484.34	280.06
1/29—1	678.52	83.40	39.31	17.26	27.71	1.61	36.20	21.04	0.088	−240.22	−3.96	1545
1/29—2	812.72	34.90	43.31	18.76	30.76	1.64	40.56	22.76	0.065	−247.68	−3.05	−1876
1/29—3	970.04	−189.44	46.36	20.92	34.92	1.67	46.54	23.60	0.051	−95.34	−0.96	2149
1/29—4	880.31	−151.73	46.13	19.08	31.58	1.65	41.94	21.92	0.048	−261.84	−2.67	2127
1/31—1	556.96	224.69	31.60	17.63	29.52	1.67	39.92	20.07	0.201	−231.98	−7.35	998.33
1/31—2	408.93	7.54	29.54	13.84	22.37	1.62	29.87	15.26	0.200	−187.13	−7.26	872.78
1/31—3	522.38	273.53	31.06	16.82	28.66	1.70	39.08	21.17	0.227	−266.82	−8.90	964.88
1/31—4	711.92	182.74	30.97	22.99	38.71	1.68	52.20	26.12	0.284	−419.24	−14.12	958.84
2/1 -1	469.94	−10230	41.50	11.32	19.75	1.74	28.76	10.53	0.036	−1698	−23.75	1723
2/1—2	562.20	−9937	42.76	13.15	23.47	1.79	34.73	11.38	0.034	−1626	−20.80	1828
2/1—3	494.88	−10617	44.49	11.12	19.67	1.77	28.90	11.41	0.029	−1613	−18.33	1979
2/1—4	477.13	−10802	43.66	10.93	18.94	1.73	27.49	10.55	0.029	−1537	−18.47	1906
2/1—5	505.95	-11,101	45.79	11.05	19.37	1.75	28.40	10.65	0.024	−1566	−16.32	2097
2/2—1	573.76	85.05	30.49	18.82	31.34	1.67	41.99	21.57	0.250	−503.64	−17.77	929.70
2/2—2	583.65	214.18	30.21	19.32	32.21	1.67	43.20	21.94	0.263	−388.73	−14.10	912.63
2/2—3	565.27	−65.70	32.33	17.48	29.59	1.69	39.97	22.59	0.207	−538.03	−15.92	1045
2/2—4	591.35	109.86	32.75	18.05	30.27	1.68	40.64	22.84	0.198	−314.49	−8.95	1073
2/5—1	686.82	249.82	39.79	17.26	28.97	1.68	38.90	21.66	0.086	−152.31	−2.42	1584
2/5—2	693.93	263.22	40.87	16.98	28.62	1.69	38.61	21.33	0.077	−113.36	−1.66	1670
2/5—3	789.99	121.17	43.98	17.96	30.54	1.70	41.54	20.50	0.055	−71.47	−0.84	1931
2/5—4	741.37	301.88	47.03	15.76	26.53	1.68	36.06	18.13	0.037	−152.69	−1.47	2212
2/5—5	858.77	158.65	46.77	18.36	31.38	1.70	42.90	20.38	0.043	−138.59	−1.35	2187
2/6—1	497.45	−8183	39.02	12.75	23.25	1.82	34.10	14.16	0.061	−1930	−32.48	1523
2/6—2	493.57	−9129	41.40	11.92	21.47	1.80	31.41	13.63	0.046	−1780	−25.09	1714
2/6—3	606.51	−11829	46.18	13.13	22.91	1.74	33.21	11.89	0.026	−1675	−17.01	2132
2/6—4	596.70	-12289	47.22	12.64	22.06	1.75	32.00	11.95	0.024	−1711	−16.25	2230
2/8—1	744.33	103.57	42.43	17.54	32.43	1.85	46.96	23.25	0.072	−149.90	−1.96	1800
2/8—2	946.33	−113.79	46.98	20.14	37.32	1.85	54.21	25.59	0.0525	−238.56	−2.30	2207
2/8—3	897.31	−226.73	52.26	17.17	31.75	1.85	46.42	22.36	0.03	−145.54	−1.02	2732
2/8—4	960.56	128.11	54.65	17.58	32.38	1.84	47.21	24.14	0.027	18.98	0.12	2987
2/8—5	957.99	88.40	52.10	18.39	34.05	1.85	49.55	25.01	0.034	−150.57	−1.06	2714
2/9—1	1421	20.01	68.17	20.84	39.06	1.87	56.94	27.18	0.013	−389.96	−1.23	4647

Table 7 (continued)

Date month/day—(number of sample)	Peak (μV)	Mean (μV)	RMS (μV)	Crest factor (–)	Impulse factor (–)	Shape factor (–)	Clearance factor (–)	Kurtosis (–)	Kurtosis factor $(\mu V)^{-4}$	Skewness (–)	Skewness factor $(\mu V)^{-3}$	energy $(\mu V)^2$
2/9—2	1249	87.05	66.22	18.87	34.02	1.80	48.90	21.92	0.011	−83.07	−0.29	4385
2/9—3	1019	96.89	65.66	15.52	28.07	1.81	40.28	21.57	0.012	−101.94	−0.36	4311
2/9—4	1612	−48.56	63.42	25.42	47.21	1.86	68.04	32.13	0.020	−501.58	−1.97	4023
2/9—5	1151	242.73	63.48	18.14	32.97	1.82	47.24	23.11	0.014	−168.33	−0.66	4030
2/10—1	524.75	−17.21	32.90	15.95	27.37	1.72	37.33	21.52	0.184	−297.37	−8.35	1083
2/10—2	548.66	−123.07	34.63	15.84	26.67	1.68	36.25	18.79	0.131	−231.58	−5.58	1199
2/10—3	792.36	−152.30	36.55	21.68	37.29	1.72	51.08	21.91	0.123	−255.87	−5.24	1332
2/10—4	609.93	−264.24	37.12	16.43	27.85	1.70	37.95	19.38	0.102	−370.09	−7.24	1378
2/10—5	664.29	−408.52	39.10	16.99	29.72	1.75	40.96	23.98	0.103	−777.28	−13.00	1529
2/13—1	557.95	155.04	28.78	19.38	33.45	1.73	46.05	23.33	0.340	−168.74	−7.08	828.53
2/13—2	573.76	96.96	32.02	17.92	31.66	1.77	44.10	24.18	0.230	−343.58	−10.46	1025
2/13—3	579.50	−75.44	33.26	17.42	30.12	1.73	41.78	20.37	0.166	−310.16	−8.43	1106
2/13—4	568.03	224.85	34.50	16.46	28.36	1.72	39.31	19.32	0.136	−360.40	−8.78	1190
2/13—5	815.09	284.57	32.14	25.36	44.17	1.74	61.26	23.61	0.221	−191.99	−5.78	1033
2/13—6	628.12	235.77	32.89	19.10	33.26	1.74	46.08	22.33	0.191	−443.64	−12.47	1082
2/14—1	763.11	635.62	28.99	26.32	48.14	1.83	68.59	27.07	0.383	−0.203	−0.008	840.74
2/14—2	657.17	500.29	31.26	21.03	37.98	1.81	54.12	24.13	0.253	−99.23	−3.25	976.92
2/14—3	649.46	630.00	35.51	18.29	32.84	1.80	47.12	21.27	0.134	−50.39	−1.13	1261
2/14—4	634.84	616.41	35.38	17.94	32.95	1.84	47.53	24.03	0.153	−37.35	−0.84	1252
2/14—5	821.41	743.39	32.98	24.91	44.65	1.79	63.68	23.50	0.199	−74.21	−2.07	1087
2/16—1	683.32	−12354	43.77	15.61	28.17	1.80	42.30	12.28	0.033	−1947	−23.21	1916
2/16—2	663.89	−14020	46.68	14.22	25.36	1.78	38.01	10.99	0.023	−1833	−18.02	2179
2/16—3	736.69	−15197	49.96	14.75	25.96	1.76	38.61	11.42	0.018	−1752	−14.05	24.96
2/16—4	886.45	−16353	51.71	17.14	29.75	1.74	43.96	11.73	0.016	−1587	−11.48	2674
2/16—5	556.45	−15419	49.20	11.31	19.50	1.72	28.64	9.89	0.017	−1616	−13.56	2421

Table 8 Mean value and Std for some factors of Table 6

Date month/day	M. Peak (μV)	S. Peak (μV)	M. Mean (μV)	S. Mean (μV)	M. RMS (μV)	S. RMS (μV)	M. Crest factor (–)	S. Crest factor (–)	M. Impulse factor (–)	S. Impulse factor (–)	M. Shape factor (–)	S. Shape factor (–)	M. Clearance factor (–)	S. Clearance factor (–)	M. Kurtosis (–)	S. Kurtosis (–)
1/8	473.09	139.95	64.83	16.58	17.04	4.86	28.23	3.07	55.3	6.06	1.957	0.075	75.80	8.57	72.26	16.62
1/11	1442	402.35	161.48	132.45	44.42	15.59	35.59	13.86	77.35	30.82	2.171	0.22	109.44	43.29	127.81	63.24
1/12	2452	410.59	417.52	116.36	67.50	2.97	36.32	5.86	95.40	16.15	2.622	0.076	149.26	25.22	151.61	40.04
1/15	690.55	1165	−19.75	328.82	22.73	27.50	19.98	11.12	39.52	37.02	1.74	0.541	56.51	60.58	53.34	84.21
1/16	322.24	106.33	−170.45	30.33	11.82	0.67	27.49	10.36	40.33	14.49	1.46	0.0182	50.82	17.97	20.85	9.96
1/17	331.53	55.50	323.06	101.99	18.88	2.22	17.53	1.51	28.51	2.93	1.63	0.0669	37.35	4.24	24.84	3.05
1/18	311.94	17.95	−27.29	57.47	15.43	0.79	20.27	1.94	30.67	3.03	1.512	0.005	39.21	3.90	16.81	2.92
1/19	577.18	440.17	496.67	99.42	26.09	0.95	21.90	16.26	32.46	24.57	1.472	0.019	41.47	31.47	24.38	31.34
1/25	439.60	109.94	377.25	80.79	27.97	7.49	17.20	2.04	27.00	3.62	1.57	0.049	35.32	5.016	15.89	2.64
1/29	627.17	81.50	315.85	68.86	36.97	6.15	17.26	3.34	28.01	4.83	1.63	0.041	37.43	6.06	16.56	0.78
1/31	970.18	284.45	319.64	104.71	50.31	4.47	19.17	4.55	32.83	7.75	1.71	0.008	45.74	10.73	18.97	1.31
2/1	800.62	96.44	112.56	53.79	50.46	2.65	19.11	6.53	28.86	2.14	1.82	0.017	41.65	3.25	21.66	1.36
2/2	921.35	193.24	471.58	88.77	47.21	3.75	19.56	3.89	31.73	6.51	1.62	0.024	42.14	8.70	19.73	3.19
2/5	679.21	15.62	461.58	18.38	69.87	12.63	10.05	2.42	13.47	3.32	1.34	0.006	16.47	4.07	5.25	0.48
2/6	532.85	116.53	−166.88	38.22	42.08	3.13	12.56	1.81	18.02	2.59	1.44	0.031	22.89	3.29	8.35	1.44
2/8	704.21	93.83	172.74	87.36	45.90	5.63	15.37	1.21	25.42	2.08	1.65	0.017	34.39	2.88	17.64	1.14
2/9	933.08	259.68	178.28	142.08	49.93	3.26	18.61	4.59	25.11	7.73	1.65	0.026	41.45	10.97	18.94	3.27
2/10	500.60	76.65	245.62	74.43	39.74	2.38	12.62	1.94	18.54	2.95	1.46	0.009	23.87	3.84	8.90	0.67
2/13	659.01	82.28	242.98	89.74	33.92	5.27	19.66	2.73	32.62	5.20	1.66	0.05	44.14	7.67	19.79	2.55
2/14	899.71	196.14	616.16	70.54	43.20	2.04	20.75	3.91	33.12	6.18	1.60	0.019	43.91	8.13	17.93	3.15
2/16	1108	77.70	212.82	164.41	63.46	3.18	17.47	1.01	29.43	1.99	1.68	0.036	39.83	2.84	21.94	2.66

Table 9 Mean value and Std for some factors of Table 7

Date month/day	M. Peak (μV)	S. Peak (μV)	M. Mean (μV)	S. Mean (μV)	M. RMS (μV)	S. RMS (μV)	M. Crest factor (–)	S. Crest factor (–)	M. Impulse factor (–)	S. Impulse factor (–)	M. Shape factor (–)	S. Shape factor (–)	M. Clearance factor (–)	S. Clearance factor (–)	M. Kurtosis (–)	S. Kurtosis (–)
1/8	227.89	259.08	82.58	34.07	14.18	0.91	30.18	0.25	45.65	0.88	1.51	0.042	57.78	1.58	44.61	10.60
1/11	201.76	19.45	−757.10	42.49	13.67	0.91	14.74	0.47	16.42	2.51	1.37	0.015	24.64	1.07	8.73	1.13
1/12	407.78	54.44	180.25	41.28	14.13	1.51	28.86	3.03	44.72	5.23	1.55	0.051	56.05	6.70	48.40	12.31
1/15	437.99	119.93	−175.14	61.16	16.44	2.48	26.21	3.88	38.97	5.56	1.49	0.021	48.70	6.73	30.79	4.69
1/16	446.29	39.98	−188.62	97.45	19.19	0.48	23.27	2.16	35.95	3.67	1.54	0.019	45.16	4.76	36.47	4.16
1/17	438.18	89.71	152.95	39.60	15.88	0.44	27.64	5.95	42.22	9.07	1.53	0.032	53.03	11.36	41.13	9.79
1/18	873.66	199.36	−2407	375.93	23.79	2.19	36.69	7.68	75.50	16.81	2.05	0.079	108.10	24.25	94.31	34.99
1/19	420.02	55.59	−1390	184.99	17.90	0.57	23.51	3.40	41.60	6.07	1.77	0.027	55.43	8.03	38.14	5.01
1/25	370.10	88.11	−1051	123.65	17.99	1.26	20.73	5.78	36.25	10.49	1.75	0.024	49.54	14.35	27.24	6.15
1/29	835.40	122.84	−55.72	134.99	43.78	3.29	19.01	1.50	31.24	2.96	1.64	0.025	41.31	4.26	22.33	1.1
1/31	550.05	125.07	172.13	115.83	30.79	0.88	17.82	3.81	29.82	6.73	1.67	0.034	40.27	9.17	20.66	4.46
2/1	502.02	36.53	−10537	460.70	43.64	1.64	11.51	0.93	20.24	1.83	1.76	0.024	29.66	2.89	10.90	0.45
2/2	578.51	11.39	85.85	115.49	31.45	1.28	18.42	0.81	30.85	1.16	1.68	0.009	41.45	1.44	22.23	0.58
2/5	754.18	71.68	218.95	75.81	43.69	3.31	17.26	1.00	29.21	1.88	1.69	0.01	39.60	2.68	20.40	1.38
2/6	548.56	61.41	−10358	2011	43.46	3.89	12.61	0.51	22.42	0.81	1.78	0.039	32.68	1.21	12.91	1.16
2/8	901.30	91.39	−4.09	157.50	49.68	4.93	18.16	1.19	33.59	2.25	1.85	0.004	48.87	3.22	24.07	1.30
2/9	1290	231.99	79.62	108.33	65.39	2.00	19.76	3.69	36.27	7.26	1.83	0.031	52.28	10.62	25.18	4.48
2/10	628	106.79	−193.07	149.14	36.06	2.38	17.38	2.45	29.78	4.35	1.71	0.026	40.71	6.05	21.12	2.09
2/13	620.41	98.44	153.63	130.12	32.27	1.93	19.27	3.17	33.50	5.57	1.74	0.017	46.43	7.72	22.19	1.94
2/14	705.20	82.50	625.14	86.28	32.82	2.78	21.70	3.80	39.31	6.90	1.81	0.021	56.21	9.64	24	2.07
2/16	705.36	120.58	−14669	1538	48.26	3.10	14.61	2.15	25.75	3.91	1.76	0.032	38.30	5.95	11.26	0.90

References

1. Li X, et al. Feature extraction using parameterized multisynchrosqueezing transform. IEEE Sens J. 2022;22(14):14263–72. https://doi.org/10.1109/JSEN.2022.3179165.
2. Scheeren B, Kaminski ML, Pahlavan L. Evaluation of ultrasonic stress wave transmission in cylindrical roller bearings for acoustic emission condition monitoring. Sensors. 2022;22(4):1500. https://doi.org/10.3390/s22041500.
3. Mirmahdi E. Modeling and effect of ultrasonic waves on bearing shells in industry by non-destructive testing. Russ J Nondestr Test. 2020;56:853–63. https://doi.org/10.1134/S1061830920100058.
4. Liu Z-X, et al. Study on the rotational speed of bearing cage based on ultrasonic measurement. Proc Inst Mech Eng Part K J Multi-body Dyn. 2017;231(4):684–9. https://doi.org/10.1177/1464419317697855.
5. Dou P, et al. Review of ultrasonic-based technology for oil film thickness measurement in lubrication. Tribol Int. 2022;165:107290. https://doi.org/10.1016/j.triboint.2021.107290.
6. Mirmahdi E, et al. Experimental investigation of bearing inner and outer wall defects by ultrasonic waves. Int J Manuf Mater Process. 2021;7(1):30–5. https://doi.org/10.37628/ijmmp.v7i1.1273.
7. Verellen T, et al. Beamforming applied to ultrasound analysis in detection of bearing defects. Sensors. 2021;21(20):6803. https://doi.org/10.3390/s21206803.
8. Mobki H. Analysis of high frequency component of ultrasound signal for fault evaluation and condition monitoring of ball bearing in induction machine. J Fail Anal Prev. 2023. https://doi.org/10.1007/s11668-023-01790-w.
9. Šiniković G, et al. Rolling bearing fault detection in the range of ultrasound. Tehnički vjesnik. 2023;30(3):830–6. https://doi.org/10.17559/TV-20220919121221.
10. Alousif A, Alali S. Machinery fault detection through ultrasound technology. In SPE Middle East Oil and Gas Show and Conference. 2021. SPE. https://doi.org/10.2118/204812-MS.
11. Garcia Marquez FP, Gomez Munoz CQ. A new approach for fault detection, location and diagnosis by ultrasonic testing. Energies. 2020;13(5):1192. https://doi.org/10.3390/en13051192.
12. Vishwakarma M, et al. Vibration analysis & condition monitoring for rotating machines: a review. Mater Today Proc. 2017;4(2):2659–64. https://doi.org/10.1016/j.matpr.2017.02.140.
13. Janssens O, Loccufier M, Van Hoecke S. Thermal imaging and vibration-based multisensor fault detection for rotating machinery. IEEE Trans Industr Inf. 2018;15(1):434–44. https://doi.org/10.1109/TII.2018.2873175.
14. Song L, Wang H, Chen P. Vibration-based intelligent fault diagnosis for roller bearings in low-speed rotating machinery. IEEE Trans Instrum Meas. 2018;67(8):1887–99. https://doi.org/10.1109/TIM.2018.2806984.
15. McDonald GL, Zhao Q. Multipoint optimal minimum entropy deconvolution and convolution fix: application to vibration fault detection. Mech Syst Signal Process. 2017;82:461–77. https://doi.org/10.1016/j.ymssp.2016.05.036.
16. Hafezi MH, Alebrahim R, Kundu T. Peri-ultrasound for modeling linear and nonlinear ultrasonic response. Ultrasonics. 2017;80:47 57. https://doi.org/10.1016/j.ultras.2017.04.015.
17. Mendioroz A, Celorrio R, Salazar A. Ultrasound excited thermography: an efficient tool for the characterization of vertical cracks. Meas Sci Technol. 2017;28(11):112001. https://doi.org/10.1088/1361-6501/aa825a.
18. Lopez A, et al. Non-destructive testing application of radiography and ultrasound for wire and arc additive manufacturing. Addit Manuf. 2018;21:298–306. https://doi.org/10.1016/j.addma.2018.03.020.
19. Koskinen T, et al. Online nonlinear ultrasound imaging of crack closure during thermal fatigue loading. NDT and E Int. 2021;123: 102510. https://doi.org/10.1016/j.ndteint.2021.102510.
20. Patel V, Tandon N, Pandey R. Defect detection in deep groove ball bearing in presence of external vibration using envelope analysis and Duffing oscillator. Measurement. 2012;45(5):960–70. https://doi.org/10.1016/j.measurement.2012.01.047.
21. Tsao W-C, et al. An insight concept to select appropriate IMFs for envelope analysis of bearing fault diagnosis. Measurement. 2012;45(6):1489–98. https://doi.org/10.1016/j.measurement.2012.02.030.
22. Moher M, Haykin S. An introduction to analog and digital communications. 2nd ed. Hoboken: John Wiley & Sons Inc.; 2006.
23. Tan M, et al. RF and microwave photonic, fractional differentiation, integration, and Hilbert transforms based on Kerr micro-combs. In: Proc. SPIE 11713, Next-Generation Optical Communication: Components, Sub-Systems, and Systems X, 117130K. 2021. https://doi.org/10.1117/12.2584018.
24. Wei Z, et al. A novel intelligent method for bearing fault diagnosis based on affinity propagation clustering and adaptive feature selection. Knowl-Based Syst. 2017;116:1–12. https://doi.org/10.1016/j.knosys.2016.10.022.
25. Singh P, Harsha SP. Statistical and frequency analysis of vibrations signals of roller bearings using empirical mode decomposition. Proc Inst Mech Eng Part K J Multi-body Dyn. 2019;233(4):856–70. https://doi.org/10.1177/1464419319847921.